Scientific Research Publishing

Computational Chemistry, 2022, 10, 157-185
https://www.scirp.org/journal/cc
ISSN Online: 2332-5984
ISSN Print: 2332-5968

Vibrational Spectroscopic Investigations, Electronic Properties, Molecular Structure and Quantum Mechanical Study of an Antifolate Drug: Pyrimethamine

Pélagie Manwal A Mekoung[1,2], Bel Youssouf G. Mountessou[2], Maraf B. Mbah[2], Martin Signe[1], Auguste Abouem A Zintchem[2], Charles P. N. Nanseu[1], Ibrahim N. Mbouombouo[2*]

[1]Department of Inorganic Chemistry, Faculty of Science, University of Yaoundé I, Yaoundé, Cameroon
[2]Computational Chemistry Laboratory, Department of Chemistry, Higher Teacher Training College, University of Yaoundé I, Yaoundé, Cameroon
Email: *indassa@yahoo.fr

How to cite this paper: Mekoung, P.M.A, Mountessou, B.Y.G., Mbah, M.B., Signe, M., Zintchem, A.A.A, Nanseu, C.P.N. and Mbouombouo, I.N. (2022) Vibrational Spectroscopic Investigations, Electronic Properties, Molecular Structure and Quantum Mechanical Study of an Antifolate Drug: Pyrimethamine. *Computational Chemistry*, **10**, 157-185.
https://doi.org/10.4236/cc.2022.104008

Received: August 4, 2022
Accepted: September 6, 2022
Published: September 9, 2022

Abstract

The computational modelling supported by experimental results can explain the molecular structure, vibrational assignments, reactive sites and several structural properties. In this context, the spectroscopic (FT-IR, FT-Raman and NMR) analysis, electronic properties (HOMO and LUMO energies) and molecular structure of pyrimethamine (Pyr) were investigated by density functional theory (DFT) method associated with three levels of theory *viz.*, B3LYP, MN15 and wB97XD with 6-311++G(d,p) and def2TZVPP as basis sets, respectively in the Gaussian 16 programs. The ^{1}H and ^{13}C NMR chemical shifts were calculated with a gauge-independent atomic orbital (GIAO) approach by also applying the same levels of theory and basis sets. All experimental results were compared with theoretical data. Although the results revealed high degrees of correlation between the theoretical and experimental values for spectroscopic properties using the three methods. Furthermore, the atomic and natural charges, energy band gap and chemical reactivity were determined, while the frontier molecular orbital (FMO) and molecular electrostatic potential (MEP) surfaces were plotted to explain the reactive nature of the title molecule.

Keywords

Electronic Property, NMR, Pyrimethamine, Vibrational Spectrum

1. Introduction

Antifolate drugs (also known as folate antagonists or folic acid antagonists) con-

stitute an important class of chemotherapeutic agents used in the treatment of cancer and microbial infections, including those of bacterial and protozoal origins [1]. Among the protozoan infectious diseases, malaria is the most important one against which antifolate drugs are administrated [2] [3]. Pyrimethamine (Pyr) [5-(4-chlorophenyl)-6-ethylpyrimidine-2,4-diamine] has been a popular antifolate drug used for the prevention and treatment of malaria as it inhibits the enzyme dihydrofolate reductase [4] [5], but the bacteria resistance with this drug has been noted. Like most antifolates, pyrimethamine contains a 2,4-diaminopyrimidine group and a phenyl ring, separated by one rotatable bond [6]. Previous theoretical and structural studies revealed that the relative orientation of the two rings and the protonation state of the 2,4-diaminopyrimidine group play a key role in drug binding [7] [8]. It is noteworthy that investigations on the antimalarial drug Pyr and its derivatives have been carried out in recent years [9]-[14]. In these investigations, the knowledge of the nature of interaction between the drugs with proteins in order to determine active sites of the template molecule has been carried out using computational methods. One of these methods includes the density functional theory (DFT) which has seen explosive growth in its application to molecular systems that are of interest in a variety of scientific fields [15]. DFT plays particularly useful roles in biological molecules as it finds application in the form of hybrid quantum mechanics and molecular mechanics [16]. Moreover, owing to its balanced accuracy and efficiency, the reliability of DFT methods [17] is helpful to economically predict compound properties and to insightfully clarify some experimental phenomena [18] [19].

As the X-ray crystallography of Pyr has been elucidated by Sethuraman *et al.* [20] [21], the present study aimed to compare DFT results with the experimental data of bond lengths, angles, torsion, NMR and to characterize its structure using energetic data. However, the experimental ^{1}H NMR data [9] were found in the literature. The structure of Pyr was optimized in gas phase using DFT under B3LYP [22] [23]/6-311++G(d,p), MN15 [24]/def2TZVPP [25] and wB97X-D [26]/def2TZVPP levels. The results were compared with their corresponding experimental values. We further extended our theoretical calculations on the molecular electrostatic potential (MEP) and Mulliken charges of Pyr.

2. Materials and Methods

2.1. Sample and Experimental Details

The pure sample (pyrimethamine) was sourced from the European directorate for the quality of medicines & healthcare (EDQM) with a degree of purity of 99.5%. The FT-IR spectrum of the title molecule was measured in the 4000 - 400 cm^{-1} region at a resolution of 1 cm^{-1}, using a PerkinElmer 2000 FT-IR spectrophotometer, vacuum in KBr pellet technique (solid phase). The FT-Raman spectrum of the molecule was also recorded using 1064 nm as excitation wavelength in the region 4000 - 100 cm^{-1} on a Bruker FT-Raman instrument. The sample was dissolved in the hexadeteurated dimethyl sulfoxide (DMSO-d_6) solvent and,

the ^{13}C NMR spectrum was recorded on a Bruker Advance 600 MHz spectrometer.

2.2. Computational Details

In the present study, we used the following functionals of the density functional theory (DFT) associated with 6-311++G(d,p) and def2TZVPP [25] basis sets:

- Hybrid density functional named Becke's three-parameter hybrid model with the Lee-Yang-Parr correlation functional (B3LYP [22] [23]);
- A Kohn-Sham global-hybrid exchange-correlation density functional *viz.*, MN15 [24];
- The long-range corrected (LC) hybrid density functional [27] [28] [29] namely wB97X-D [26].

All calculations were performed using Gaussian 16 software package [30] and GaussView visualization program [31]; their output files were analysed with GaussSum program [32]. The optimized structural parameters were used in the vibrational frequencies (IR, Raman), isotropic chemical shifts (NMR). The vibrational frequencies, IR and Raman intensities for pyrimethamine were calculated at B3LYP/6-311++G(d,p), wB97XD/def2TZVPP and MN15/def2TZVPP methods. Computed harmonic frequencies were scaled by a factor of 0.967 (B3LYP) [33], 0.955 (wB97XD) [34] and 0.977 (MN15) obtained from the following formula as reported by Malloum *et al.* [35] in order to improve the agreement with the experimental results:

$$\lambda = \frac{\sum_{i=1}^{N} \omega_i^h \nu_i^{\exp}}{\sum_{i=1}^{N} \left(\omega_i^h\right)^2}$$

(where $\nu_i^{\exp}$ stands for the i^{th} experimental frequency corresponding to the harmonic calculated ω_i^h frequency. N is the number of frequencies investigated).

The total energy distribution (TED) was calculated using VEDA program [36] in order to characterize the fundamental vibrational modes. ^{1}H and ^{13}C NMR chemical shifts were evaluated using the gauge-independent atomic orbital (GIAO) approach [37] by applying the three corresponding methods used in this work. In addition, the frontier molecular orbitals (FMOs), the molecular electrostatic potential (MEP), and the Mulliken population analysis of pyrimethamine were also theoretically investigated.

3. Results and Discussion

3.1. Potential Energy Surface (PES) Scan

The pyrimethamine (Pyr) molecule has one ethyl group and two amino substituents attached to the pyrimidine ring. The ethyl (C_2H_5), methyl (CH_3) and amino (NH_2) groups were chosen to examine the possible conformers of the molecule under investigation. Sethuraman *et al.* [20] study shows that pyr has two conformers (A and B). In order to determine conformational flexibility of

Pyr, the potential energy surface scans was achieved with B3LYP/6-311++G(d,p) method by varying the dihedral angle D1 (C12-C13-C16-C19), D2 (C13-C16-C19-H22) and D3 (N30-C15-N26-H27) in 36 steps of size 10˚. The resultant energy profiles are shown in Figures 1-3, respectively. The structures of the possible conformers and their energies are given in Table 1. It can be seen from Table 1 that structures S3, C2 and M3 have the same minimum energy (−1144.567789 a.u) for the different selected dihedral angles, suggesting that they represent the same conformer. It corresponds to the most stable conformer. According to X-ray crystallographic study, it is the molecule A. In this study, calculations were done for the most stable conformer.

3.2. Molecular Geometry

The X-ray study of pyrimethamine whose chemical structure is depicted in Figure 4(a) was elucidated by Sethuraman *et al.* [20] [21] The structure of pyrimethamine was optimized (Figure 4(b)) at B3LYP/6-311++G(d,p), MN15/def2TZVPP and wB97XD/def2TZVPP levels of theory. The results of the selected optimized structure parameters (bond lengths, bond angles, dihedral angle) were compared with their corresponding experimental values in Table 2.

The bond connecting the pyrimidine and phenyl rings namely C4-C12 (b) is predicted at 1.492 Å for B3LYP, 1.484 Å for MN15 and 1.485 Å for wB97XD

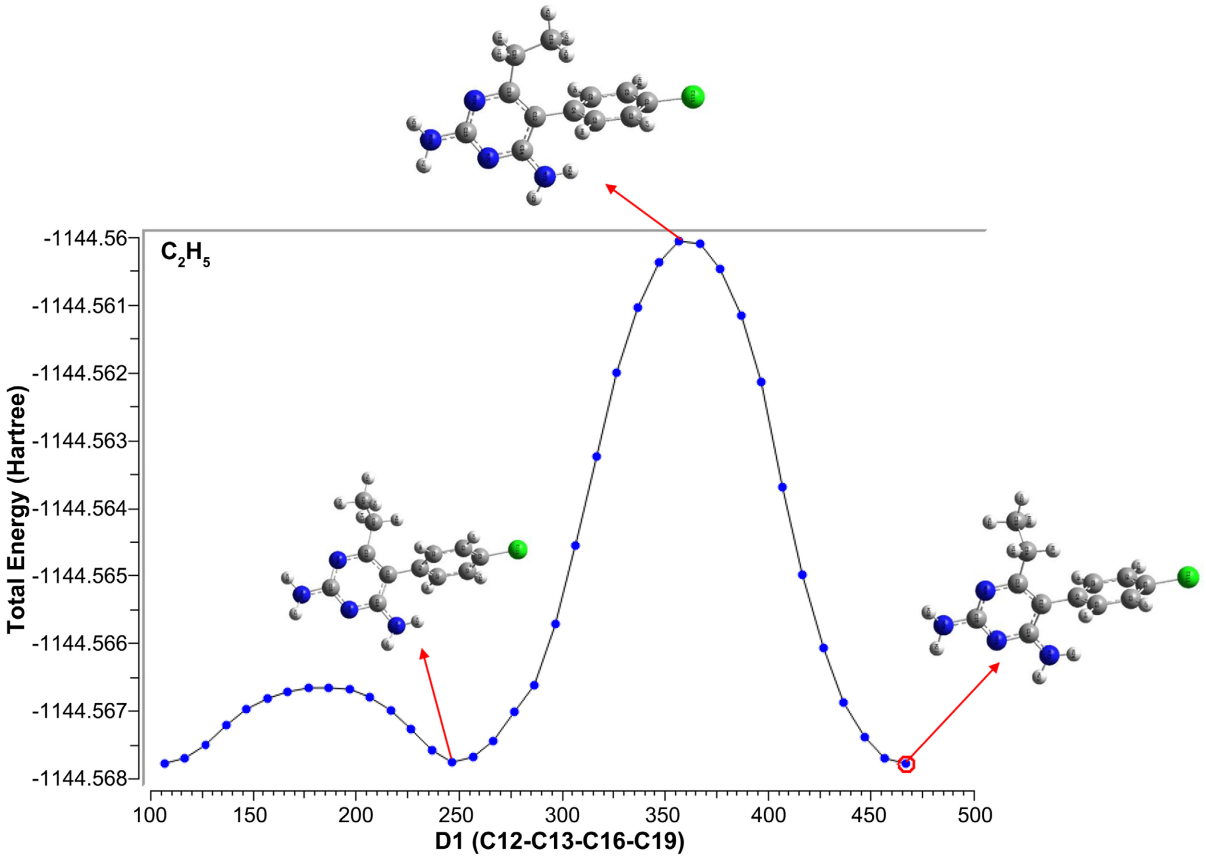

Figure 1. Potential energy surface scan for dihedral angle D1 (C12-C13-C16-C19).

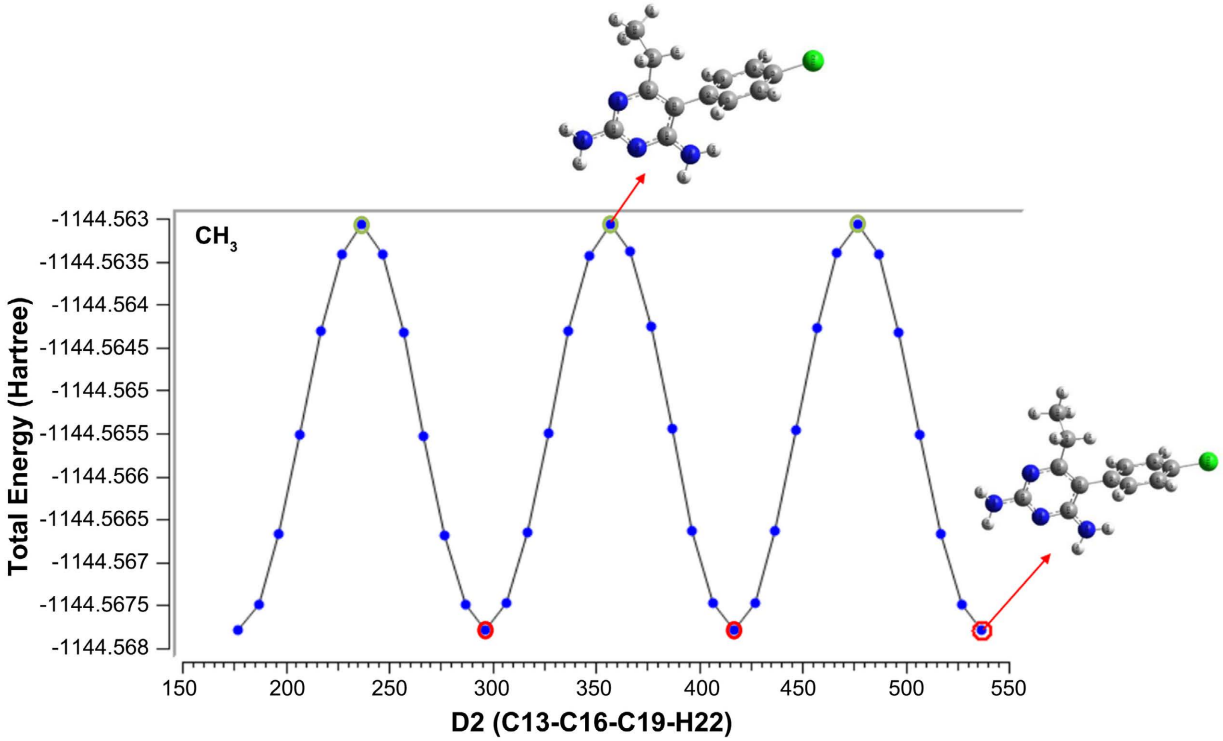

Figure 2. Potential energy surface scan for dihedral angle D2 (C13-C16-C19-H22).

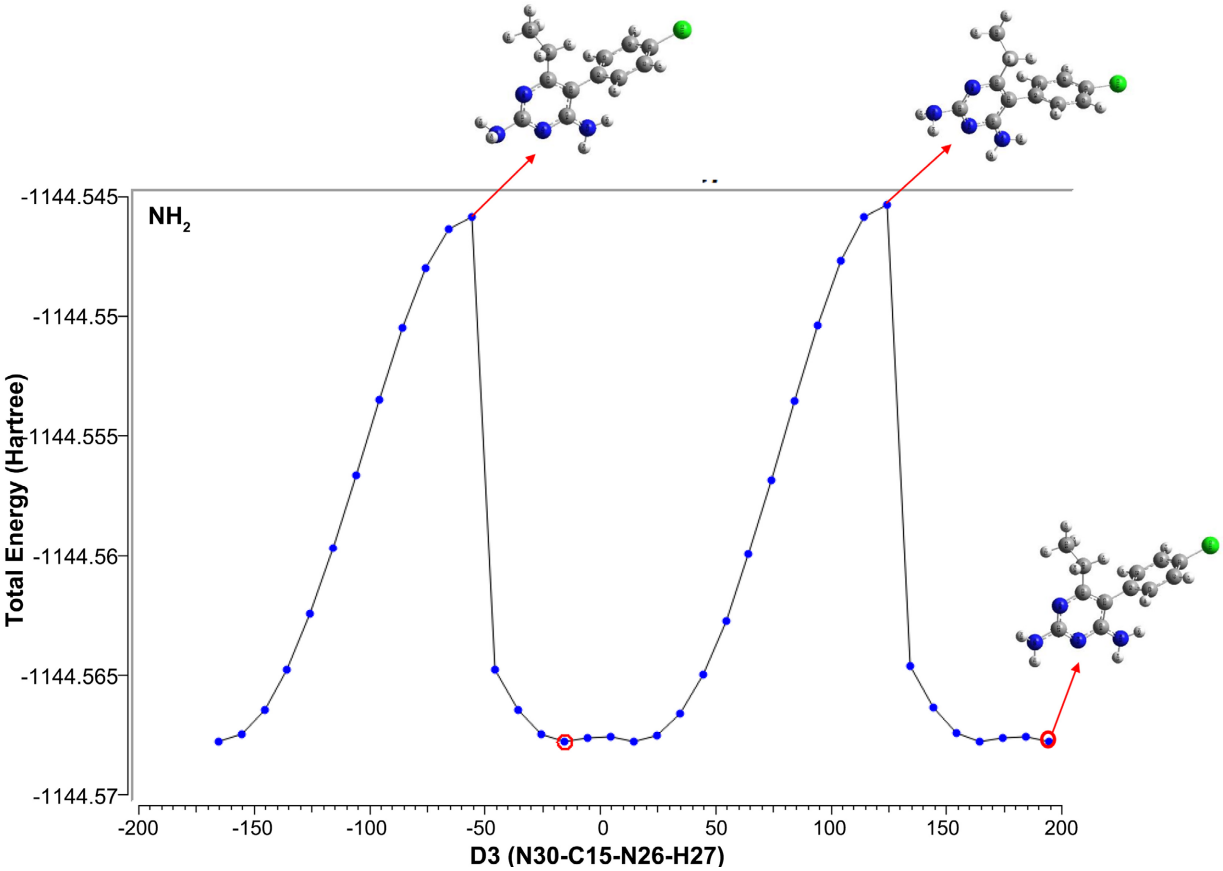

Figure 3. Potential energy surface scan for dihedral angle D3 (N30-C15-N26-H27).

Table 1. Theoretical possible structures for selected dihedral angles of pyrimethamine.

C_2H_5	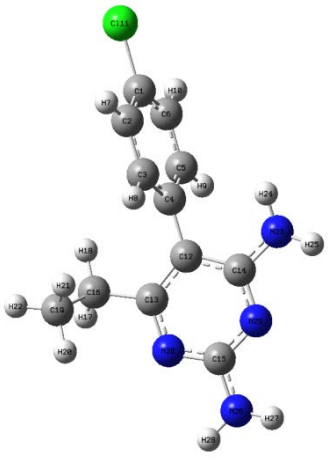	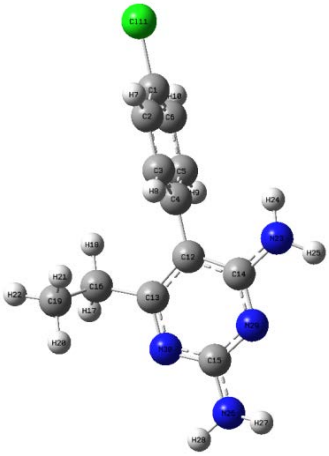	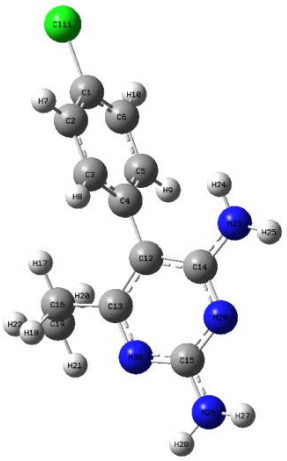
	S1	**S2**	**S3**
Energy (a.u)	−1144.567756	−1144.560062	**−1144.567789**
CH_3	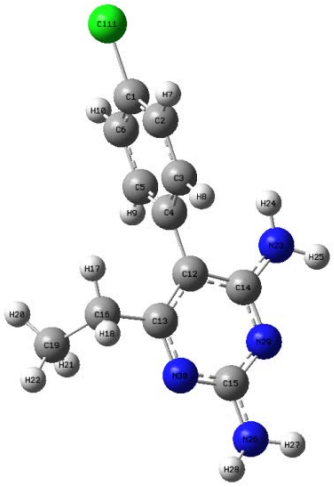	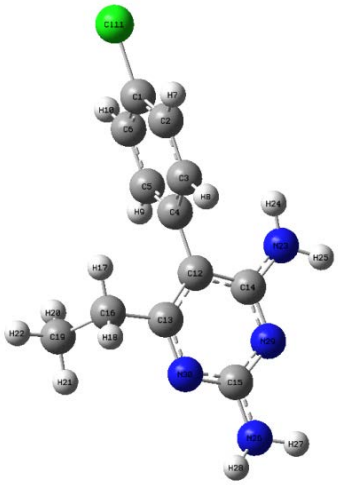	
	C1	**C2**	
Energy (a.u)	−1144.563074 a.u	**−1144.567789**	
NH_2	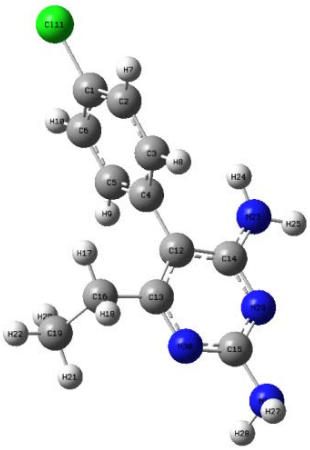	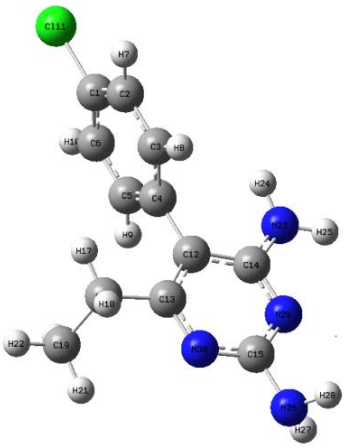	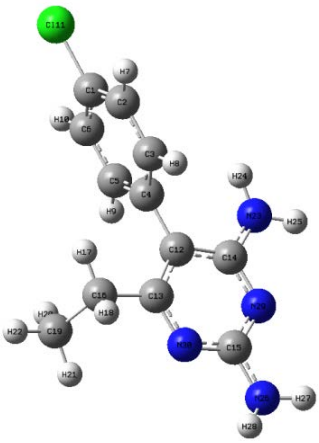
	M1	**M2**	**M3**
Energy (a.u)	−1144.545873	−1144.545363	**−1144.567789**

Table 2. Selected experimental values and theoretical optimized structure parameters of pyrimethamine under B3LYP/6-311++G(d,p), MN15/def2TZVPP and wB97X-D/def2TZVPP levels.

Geometric parameters	Experimental values[a]	B3LYP/6-311++G(d,p)	MN15/def2TZVPP	wB97XD/def2TZVPP
		Bond length (Å)		
C1-Cl11	1.742 (2)	1.759	1.726	1.737
N30-C13	1.349 (2)	1.343	1.336	1.335
N30-C15	1.338 (3)	1.337	1.335	1.331
N26-C15	1.355 (3)	1.369	1.360	1.360
N29-C15	1.338 (3)	1.339	1.335	1.333
N29-C14	1.339 (3)	1.335	1.330	1.328
N23-C14	1.340 (3)	1.367	1.362	1.358
C4-C12	1.491 (3)	1.492	1.484	1.485
***r**	-	0.994	0.994	0.995
		Bond angles (˚)		
C15-N30- C13	116.3 (18)	116.7	116.6	116.5
C15-N29-C14	116.4(17)	116.4	116.5	116.3
N30-C15- N29	126.6 (18)	126.6	126.5	126.7
N30-C15-N26	116.6 (2)	116.9	116.8	116.8
N26-C15-N29	116.9 (19)	116.6	116.7	116.5
N23-C14-C12	121.0 (18)	121.4	121.2	121.2
N29-C14-C12	122.0 (19)	122.5	122.3	122.3
N29-C14-N23	117.0 (18)	116.2	116.4	116.5
N30-C13-C12	122.7 (18)	122.3	122.5	122.4
N30-C13-C16	114.8 (18)	115.0	115.6	115.6
Cl11-C1-C2	118.3 (2)	119.5	119.6	119.6
Cl11-C1-C6	120.2 (19)	119.5	119.6	119.6
***r**	-	0.97	0.98	0.98
		Dihedral angle (˚)		
C12-C13-C16-C19	97.8 (3)	107.0	83.5	90.7
C3-C4-C12-C13	73.3 (3)	81.8	69.3	82.2
C5-C4-C12-C14	74.7 (3)	81.1	67.2	80.9
C16-C13-N30-C15	178.3 (2)	178.5	175.8	177.5
R	-	0.998	0.991	0.981

*r represents the correlation coefficient between experimental and theoretical data; For numbering of atoms refer to **Figure 1**; [a]See reference [21].

methods, respectively. The theoretical torsion angles C12-C13-C16-C19, which represents the deviation of the ethyl group from the benzene plane are 107.0˚ (B3LYP), 83.5˚ (MN15) and 90.7˚ (wB97XD). These values are in close agreement with those observed in the crystal structure of pyr [(C5A-C9A = 1.491 Å), C5A-C6A-C7A-C8A = 97.8˚)].

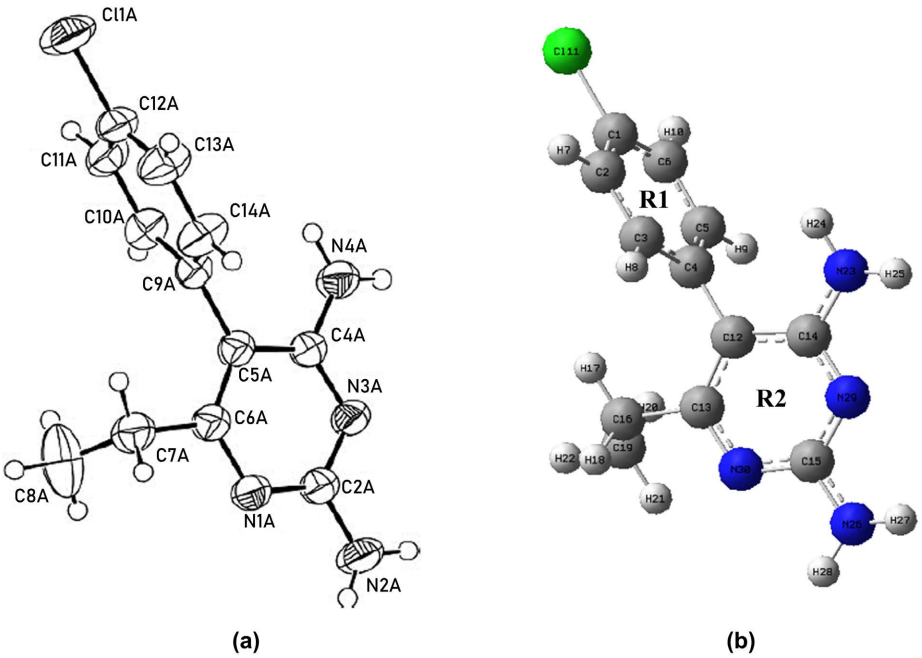

Figure 4. X-ray molecular (a) and theoretical optimized (b) structure of pyrimethamine.

The correlation coefficients (r) between experimental and theoretical bond lengths were 0.994, 0.994 and 0.995 for bond lengths and 0.97, 0.98 and 0.97 for bond angles for B3LYP, MN15 and wB97XD methods, respectively. It was worth mentioning that from correlation values, the wB97XD/def2TZVPP level gave the most accurate results than other methods for the bond lengths, while for the computations of bond angles, the best results were found by using MN15/def2TZVPP level. On the other hand, we observed a weak relationship between some experimental and theoretical parameters. It must be noted that the experimental results were obtained from the solid phase, whereas the theoretical calculations were made from the gas phase of the molecule. In the solid-state, intermolecular interactions connected the molecules together, whereas in gaseous phase, these interactions were much weaker than in the solid-state, due to permanent vibrations within the molecule. These observations allowed us to conclude that the differences between the experimental and theoretical values are normal [38] [39].

3.3. Vibrational Assignments

Vibrational frequencies have been shown to be effective in the identification of functional groups of organic compound as well as in the study of molecular conformations and kinetic reactions. The calculated and scaled up by appropriate frequency factor using B3LYP/6-311++G(d,p), MN15/def2TZVPP and wB97XD/def2TZVPP with their relative intensities, probable assignment and total energy distribution (TED) of the title molecule are summarized in **Table 3**. A complete assignment of fundamental vibrational modes was proposed based on the calculated TED value infrared and Raman intensities.

Table 3. Calculated (unscaled and scaled) frequencies, IR intensity, Raman intensity and probable assignments (characterized by TED) of pyrimethamine using B3LYP/6-311++G(d,p), MN15/def2TZVPP and wB97XD/def2TZVPP methods.

	Exp. FT-IR (cm^{-1})	Exp. FT-Raman (cm^{-1})	B3LYP/6-311++G(d.p)				MN15/def2TZVPP				wB97XD/def2TZVPP				Vibrational assignments	TED %
			Unscaled	Scaled	$^aI_{IR}$	^bR_A	Unscaled	Scaled	$^aI_{IR}$	^bR_A	Unscaled	Scaled	$^aI_{IR}$	^bR_A		
1	3468 m	3063 w	3730	3607	44.15	61.79	3788	3701	53.66	66.46	3788	3617	47.80	58.14	ν_{as}(NH2) (N26)	ν_{as}(NH2) (N26) (100)
2			3721	3598	55.61	44.29	3758	3672	65.51	46.74	3775	3605	60.76	40.72	ν_{as}(NH2) (N23)	ν_{as}(NH2) (N23) (100)
3	3310 m	-	3604	3485	76.37	273.60	3646	3562	108.06	252.22	3655	3491	87.09	220.79	ν_s(NH2) (N26)	ν_s(NH2) (N26) (99)
4			3597	3478	53.10	166.66	3624	3541	56.62	158.28	3646	3482	58.89	133.18	ν_s(NH2) (N23)	ν_s(NH2) (N23) (99)
5	3150 m	2985 vw	3199	3094	0.61	213.58	3238	3163	1.57	218.71	3229	3084	0.30	205.75	ν(C-H) R1	[ν(C2-H7), ν(C6-H10)] (**85**)
6			3198	3092	3.35	43.64	3237	3162	5.30	50.85	3228	3083	2.37	33.51	ν(C-H) R1	[ν(C2-H7), ν(C6-H10)] (**88**)
7			3176	3071	3.64	42.18	3208	3135	6.35	45.71	3205	3060	3.50	39.39	ν(C-H) R1	ν(C5-H9) (**89**)
8			3173	3068	4.32	45.08	3206	3133	5.70	44.28	3203	3059	3.77	41.49	ν(C-H) R1	ν(C3-H8) (**90**)
9	2977 w	2941 vw	3113	3010	33.70	12.17	3156	3084	36.97	16.02	3145	3004	32.35	8.44	ν_{as}CH2, ν_{as}CH3	[ν_{as}CH2 (C16), ν_{as}CH3 (C19)] (**90**)
10			3094	2991	22.15	92.38	3149	3076	36.64	121.82	3135	2994	29.05	102.99	ν_{as}CH3	ν_{as}CH3 (C19) (**82**), ν_{as}CH2 (C16) (**13**)
11			3086	2985	20.46	92.50	3132	3059	5.46	70.18	3122	2982	4.20	66.05	ν_{as}CH3	[ν(C16-H17), ν_{as}CH3 (C19)] (**88**)
12			3044	2943	12.88	119.76	3097	3026	16.47	116.98	3085	2946	13.35	113.37	ν_sCH2	ν_{as}CH3 (C19) (**12**), ν_sCH2 (C16) (**80**)
13			3028	2928	31.46	183.60	3063	2992	26.27	179.85	3054	2917	24.90	174.93	ν_sCH3	ν_sCH3 (C19) (**96**)
14	1628 vs		1639	1585	259.20	3.72	1665	1626	249.09	348.24	1675	1600	73.01	177.50	βNH2 (N23), βNH2 (N26)	[βNH2 (N23), βNH2 (N26)] (67)
15			1630	1577	586.03	6.21	1661	1622	672.54	10.91	1667	1592	820.66	39.38	βNH2 (N23), βNH2 (N26)	ν(C=C) R1 (11), [ν(N29-C14), ν(C12-C13)] (10), [βNH2 (N26), βNH2 (N23)] (41)
16			1629	1575	209.65	224.69	1634	1597	471.83	8.53	1656	1581	413.17	9.17	ν(C=C) R1	ν(C=C) R1 (21), [ν(C4-C12), ν(C5-C6)] (16), [βNH2 (N26), βNH2 (N23)] (13), β(HCC) R1 (12)
17	1560 vs	1594 s	1609	1556	160.45	45.76	1626	1589	121.53	2.41	1635	1562	43.61	1.52	ν(N=C), ν(C=C) R2	[ν(N29-C14), ν(C12-C13)] (29), [βNH2 (N26), βNH2 (N23)] (21)
18			1597	1544	4.15	2.99	1616	1579	152.39	2.21	1633	1560	185.71	1.46	ν(C=C) R1	β(HCC) R1 (10), [ν(C1-C6), ν(C4-C5)] (73)
19			1585	1533	267.91	0.89	1593	1556	163.52	5.56	1624	1551	65.71	2.18	ν(N=C), ν(C=C) R2	[ν (N30-C15), ν(C12-C13)] (47)
20			1521	1471	15.07	7.91	1536	1501	24.74	17.63	1549	1480	9.73	4.66	β (HCC) R1	β(HCC) R1 (54), β(CCC) R1 (13)
21	1439s		1510	1460	3.79	3.10	1496	1461	31.26	5.93	1515	1447	8.00	3.81	βCH3, βCH2	[βCH3 (C19), βCH2 (C16)] (69), τ(H21-C19-C16-C13) (11)
22			1496	1447	12.92	7.76	1485	1451	128.99	1.34	1505	1437	158.57	1.02	δ_{as} CH3	δ_{as}CH3 (C19) (72)
23			1487	1438	1.56	11.00	1480	1446	21.67	9.14	1503	1436	4.75	10.22	βCH2	[βCH3 (C19), βCH2 (C16)] (78)
24			1476	1427	183.84	2.08	1480	1446	111.86	19.83	1495	1428	9.80	10.45	ν(N-C) R2	[ν(N26-C15), ν(N29-C15)] (43), [βNH2 (N26), βNH2 (N23)] (17)
25	1404 w		1456	1408	264.91	25.45	1468	1434	0.24	8.36	1491	1423	258.71	11.13	ν(N-C) R2	[ν(N23-C14), ν(N29-C15)] (29), δ(N29-C15-N30) (15)
26			1430	1382	6.70	21.12	1447	1414	8.27	22.44	1459	1393	6.62	15.43	ν(N=C), ν(C=C) R2	[ν(C13-C16), ν(N30-C13), ν(C12-C13)] (44), ρCH3 (C19) (15)
27			1417	1371	5.04	0.80	1426	1393	6.38	1.36	1442	1377	5.08	0.51	β(HCC) R1	β(HCC) R1 (41), β(CCC) R1 (14), ν(C=C) R1 (14)
28			1397	1351	3.25	11.48	1388	1356	4.04	4.69	1412	1348	4.41	7.58	ρCH3	ρCH3 (C19) (76)
29			1351	1306	1.21	19.51	1334	1303	0.79	22.34	1358	1297	0.17	9.48	wCH2	δ(H18-C16-C19) (11), [βCH3 (C19), wCH2 (C16)] (10), wCH2 (56)
30	1287 m	1283 m	1322	1278	0.20	1.02	1323	1292	37.16	8.27	1333	1273	0.27	1.31	β(HCC) R1	β(HCC) R1 (84)
31			1312	1268	19.42	5.11	1311	1280	6.19	37.95	1328	1268	25.11	6.62	δ(HCC) ethyl group	δ(H18-C16-C19) (31), [ν(C12-C13), ν(N30-C13), ν(C30-C15)] (25)

Continued

32			1297	1254	9.18	37.95	1307	1277	0.63	1.34	1318	1259	8.51	44.95	ν(CC) R1	[ν(C5-C6), ν(C4-C12), ν(C4-C5), ν(C1-C6)] (46), β(CCC) R1 (12)
33			1294	1251	5.96	25.66	1299	1269	1.39	19.89	1298	1239	0.78	1.43	ν (CC)	[ν(C4-C5), ν(C2-C3), ν(C1-C2), ν (C4-C12)] (54)
34	1235vw		1263	1221	4.89	8.29	1256	1227	3.77	1.74	1275	1217	6.36	2.65	twCH2	[ν(C12-C13), ν(N30-C13), ν(C30-C15)] (19), twCH2 (C16) (19)
35			1199	1160	0.12	6.36	1183	1155	0.24	3.55	1212	1157	0.09	3.00	β(HCC) R1	ν(C=C) (R1) (10), β(HCC) (R1) (77)
36			1166	1128	13.02	8.46	1161	1134	8.56	13.23	1181	1128	10.76	6.50	ρNH2 (N23), ρNH2 (N26)	[ν(N26-C15), ν(N29-C15)] (33), [ρNH2 (N23), ρNH2 (N26)] (43)
37			1130	1093	3.55	4.30	1126	1101	61.26	38.24	1140	1089	3.53	1.92	ρCH2	[ν (C12-C13), ν (N30-C13), ν (C30-C15)] (12), τ (H20-C19-C16-C13) (10), ρCH2 (15)
38	1087 m	1086 w	1123	1086	5.92	0.46	1116	1090	7.98	0.23	1136	1085	6.35	0.16	β(HCC) R1	ν R1 (C=C) (18), β(HCC) R1 (55)
39			1103	1067	2.19	2.01	1111	1085	5.48	0.87	1128	1077	64.01	32.95	ρNH2 (N23), ρNH2 (N26)	τ (H21-C19-C16-C13) (16), [ρNH2 (N23), ρNH2 (N26)] (17)
40	1012 w		1100	1064	73.22	33.07	1099	1073	0.90	6.33	1119	1069	3.81	4.53	ν(CC) R1	[ν(C1-C6), ν(C1-C2)] (66), β(HCC) R1 (15)
41			1073	1038	5.56	8.59	1073	1048	9.74	8.88	1087	1038	7.52	7.12	twCH3	γ(C19-C16) (21), [ρNH2 (N23), ρNH2 (N26)] (15), twCH3 (13), (15)
42	988w		1041	1006	9.49	14.66	1044	1020	1.07	8.11	1058	1011	3.79	10.78	δ(CCC) R1	[δ(C1-C6-C5), δ(C1-C2-C3)] (20)
43			1027	993	20.88	0.67	1017	993	14.49	0.44	1040	994	16.78	0.45	δ(CCC) R1	[δ(CCC) R1, δ(N29-C15-N30)] (10), [δ(C1-C6-C5), δ(C1-C2-C3)] (43)
44			1017	983	28.60	7.98	1011	987	0.11	0.71	1031	984	28.09	3.56	γ(CC), ν(NC)	[γ(C13-C16), ν(C30-C13)] (19), [ρNH2 (N23), ρNH2 (N26)] (18), ν(C19-C16) (16)
45			997	964	11.08	6.23	1006	983	27.54	1.86	1016	970	0.31	0.21	γ(CC) ethyl group	[γ(N26-C15), ν(N29-C15)] (12), γ(C19-C16) (16), [δ(C13-N30-C15), δ(C14-N29-C15)] (10)
46			987	955	0.07	0.17	997	974	5.29	2.87	1013	967	9.42	4.48	τ(HCCC) R1	τ(HCCC) R1 (83), [τ(C2-C1-C6-C5), τ(C3-C2-C1-C6)] (10)
47			971	939	0.27	0.15	995	972	1.17	0.73	999	954	0.19	0.12	τ(HCCC) R1	τ(HCCC) R1 (67), τ(C1-C6-C5-C4) (23)
48			932	901	7.41	3.99	940	918	11.77	2.77	950	907	8.54	3.20	γ(CC) ethyl group	γ(C19-C16) (36)
49	833 w	852.4	847	819	37.37	0.36	869	849	38.61	0.38	872	833	35.97	0.37	τ(HCCC) R1	τ R1 (69)
50			843	815	0.59	0.76	860	840	0.52	2.96	867	828	0.51	0.36	τ(HCCC) R1	τ R1 (97)
51			825	798	18.16	0.85	840	821	16.60	0.68	855	816	18.42	0.60	τ(CNCN) R2	τ R2 (59)
52			800	774	4.57	1.44	788	770	3.72	1.91	813	777	4.10	1.16	ρCH2	[τ(H18-C16-C13-C12), τ(H22-C19-C16-C13)] (50)
53	748vw	750 m	761	736	7.52	12.50	764	747	4.44	3.16	776	742	4.01	6.46	δ(CCC) R1	[γ(Cl11-C1), ν(C1-C6), ν(C1-C2)] (12), [δ(CCC) R1, δ(N29-C15-N30)] (31), [δ(C1-C6-C5), δ(C1-C2-C3)] (12)
54	724 vw		749	725	3.59	0.31	760	743	4.61	10.91	773	738	5.52	7.70	τ(CCCC) R1	τR1 (13), τ(C1-C6-C5-C4) (24), [τ_o(C16-C12-N30-C13), τ R2] (20), [τ_o(C12-C3-C5-C4), τ(C2-C1-C6-C5), τ(C12-C13-C16-C19)] (10)
55			748	723	3.00	0.53	753	735	0.63	1.17	765	731	2.28	0.28	τ_o(CCNC) R2	τ(C1-C6-C5-C4) (15), [τ_o(C16-C12-N30-C13), τR2] (40)
56			692	669	2.38	1.23	698	682	2.90	4.04	714	682	1.90	0.53	τ_o(CCNC)	[τ_o(C16-C12-N30-C13), τ_o(N23-C12-N29-C14)] (55)
57	-	651 m	662	640	6.66	18.69	659	644	4.45	15.57	672	642	5.13	11.21	δ(NCN) R2	[γ(Cl11-C1), ν(C1-C6), ν(C1-C2)] (13), δ(N29-C15-N30) (24), [δ(C13-N30-C15), δ(N14-N29-C15)] (12)
58	-		646	625	0.02	4.39	632	618	0.07	4.77	654	625	0.01	4.38	δ(CCC) R1	[ν(C1-C6), ν(C4-C5)] (12), [δ(C1-C2-C3), δ(C1-C6-C5)] (77)
59	604w	601 m	603	583	1.25	14.59	608	594	1.47	16.35	615	587	0.90	14.94	ν(NC) R2	[ν(C12-C13), ν (N30-C13), ν(C30-C15)] (11), [γ(N23-C14), ν(N29-C15)] (15)
60	-		593	573	10.64	1.11	584	571	10.06	0.45	602	575	11.19	0.74		[δ(C4-C12-C13), δ(N23-C14-N29), δ(C16-C13-N30), δ(C14-N29-C15), δ(C13-N30-C15)] (33)
61	-		552	533	2.22	2.37	541	528	5.52	2.41	557	532	3.14	2.14	δ(CCN) R2	[γ(C13-C16), ν(C30-C13)] (12), [δ(C16-C13-N30), [δ(C13-N30-C15), δ(N23-C14-N23)] (41)

Continued

62	512 w		527	510	10.94	1.10	534	522	11.00	0.63	540	515	8.94	0.82	tw NH2 (N23)	[tw NH2 (N23), τ(C2-C1-C6-C5), τ_o(C12-C3-C5-C4)] (42)
63			513	496	31.29	2.36	524	512	16.31	1.82	526	502	26.90	1.82	tw NH2 (N23)	[tw NH2 (N26), τ(C2-C1-C6-C5), τ(C3-C2-C1-C6)] (14), [tw NH2 (N23), τ(C2-C1-C6-C5), τ_o(C12-C3-C5-C4)] (43)
64	-		491	475	3.75	0.06	501	489	9.00	0.74	506	483	2.24	0.45	twNH2 (N26)	[tw NH2 (N26), τ(C2-C1-C6-C5), τ(C3-C2-C1-C6)] (68)
65	-	475.8 vw	467	451	8.78	0.96	472	461	8.71	1.52	479	457	7.36	0.94	γ(ClC)	[γ(Cl11-C1), ν(C1-C6), ν(C1-C2)] (42)
66	-		454	439	9.63	0.57	446	436	3.12	0.67	464	443	6.05	0.70	δ(CCC) R1	δ(C12-C4-C3) (28), [tw NH2 (N23), τ(C2-C1-C6-C5), τ_o(C12-C3-C5-C4)] (12) (17), [(C4-C12-C13-N30), τ(C13-N30-C15-N29), τ_o(N26-N29-N30-C15)] (11)
67	-		420	407	0.69	0.58	421	411	0.78	2.32	427	407	0.37	0.27	τ(CCCC) R1	τR1 (HCCC) (12), [τ(C2-C1-C6-C5), τ(C3-C2-C1-C6)] (79)
68	-	357.3 m	368	356	312.11	1.27	361	353	2.82	2.14	366	350	3.99	2.66	wNH2 (N26)	twNH2 (N26) (85)
69	-		355	343	9.60	2.20	352	344	3.03	3.31	357	341	3.61	3.76	τ(CCCC) R1	[δ(C4-C12-C13), δ(N26-C15-N30)] (24), [τ(C1-C6-C5-C4), τ_o(Cl11-C2-C6-C1)] (35)
70	-		346	335	3.53	5.87	325	318	4.65	0.28	335	320	8.65	0.03	δ (NCN) R2	[δ(N23-C14-N29), δ(C14-N29-C15)] (55)
71	-		330	319	5.70	0.27	297	290	17.13	1.82	324	309	277.43	1.26	δ(NCN) R2	[δ(N26-C15-N30), δ(C16-C13-N30), δ(C13-N30-C15)] (39), [τ(H18-C16-C13-C12), τ(H22-C19-C16-C13)] (10)
72	-		305	295	149.55	2.34	287	280	149.38	1.30	305	291	24.06	1.45	wNH2 (N23), δ(CCCl11)	[δ(C2-C1-Cl11), δ(C13-C16-C19)] (27), wNH2 (N23) (37)
73	-		297	287	27.37	1.45	281	275	21.09	0.62	291	278	6.50	1.05	wNH2 (N23)	[δ(C2-C1-Cl11), δ(C13-C16-C19)] (30), wNH2 (N23) (41)
74	-		287	277	3.27	1.48	235	230	0.09	2.82	270	257	160.04	1.35	δ(CCC)	δ(C13-C16-C19) (33), [τ(C4-C12-C13-N30), τ(C13-N30-C15-N29), τ_o(N26-N29-N30-C15)] (26)
75	-	230 m	228	220	0.19	4.75	219	214	1.82	0.16	233	223	0.24	3.42	ν(CC)	[γ(C4-C12), ν(C5-C6)] (15), [βR1 (HCC), δ(N29-C15-N30)] (10), τ(H21-C19-C16-C13) (12)
76	-		216	209	6.20	0.04	211	206	4.76	3.12	221	211	5.19	0.05	τ(CNCN) R2	[τ (C13-N30-C15-N29), τ(C14-N29-C15-N29)] (80)
77	-		201	194	0.59	1.72	203	198	213.33	0.64	210	200	0.36	2.53	δ(NCN) R2	[γ(C4-C12), ν(C5-C6)] (12), [δ(N26-C15-N30), δ(C16-C13-N30), δ(C13-N30-C15)] (20)
78	-		163	158	1.42	0.35	179	175	0.39	0.41	171	164	1.85	0.47	τ(CCCN) R2	[τ(C1-C6-C5-C4), τ(Cl11-C2-C6-C1)] (11), [τ(C4-C12-C13-N30), [τ(C13-N30-C15-N29), τ_o(N26-N29-N30-C15)] (14)
79	-		152	147	1.42	0.26	148	145	0.96	0.35	155	148	1.30	0.29	τ(CCCN) R2	[τ(C4-C12-C13-N30), τ(C13-N30-C15-N29), τ_o(N26-N29-N30-C15)] (14)
80	-	102 vs	111	107	0.68	0.83	109	107	1.42	1.01	108	104	0.70	0.75	τ_o(CCNC) R2	δ(C12-C4-C3) (12), [δ(C2-C1-Cl11), δ(C13-C16-C19)] (11), [τ_o(C16-C12-N30-C13), τ(C4-C12-C13-N30), τ(C12-C13-N30-C15), τ(C13-N30-C15-N29)] (50)
81	-		51	50	0.18	0.97	61	60	0.46	1.86	62	59	0.24	1.00	τ_o(CCCC)	[τ_o(C12-C3-C5-C4), τ(C3-C2-C1-C6), τ(C12-C13-C16-C19)] (43), [τ_o(C12-C3-C5-C4), τ(C2-C1-C6-C5), τ(C12-C13-C16-C19)] (13)
82	/		47	46	0.21	2.20	49	48	0.18	4.48	49	47	0.04	2.01	τ(CCCN) R2	[τ(C4-C12-C13-N30), τ(C13-N30-C15-N29)] (63)
83	-		35	34	0.08	1.67	49	48	0.10	4.62	42	40	0.09	1.72	τ_o(CCCC)	[τ_o(C12-C3-C5-C4), τ(C3-C2-C1-C6), τ(C12-C13-C16-C19)] (17), [τ_o(C12-C3-C5-C4), τ (C2-C1-C6-C5), τ(C12-C13-C16-C19)] (51)
84	-		21	20	0.11	8.61	38	37	0.20	3.23	18	17	0.09	7.61	τ(CCCC)	τ(C13-C12-C4-C5) (89)

ν_s, very strong; s, strong; m, medium; w, weak; vw, very weak; [a]I_{IR}: IR intensities (Km/Mol), [b]RA: Raman scattering activity (A^4/AMU), ν: stretching; β: deformation in the plane; γ: deformation out-of-plane; w: wagging; τ: torsion, βR: deformation ring, τ_R: torsion ring, ρ: rocking, tw: twisting, δ: deformation, R1: phenyl ring, R2: pyrimidine ring.

The title molecule had 30 atoms, which underwent 84 (3N-6) normal modes of vibrations, 29 modes of vibrations were stretching, 28 modes of vibrations in plane bending and remaining 27 modes of vibrations were torsion. It agreed with C1 point group symmetry, all vibrations were active in Raman and IR absorptions. The experimental FT-IR and FT-Raman spectra are compared with corresponding predicted spectra in **Figure 5** and **Figure 6** respectively. The theoretical infrared and Raman spectra of pyrimethamine are presented in **Figure S1** and **Figure S2** (**Supplementary Material**), respectively.

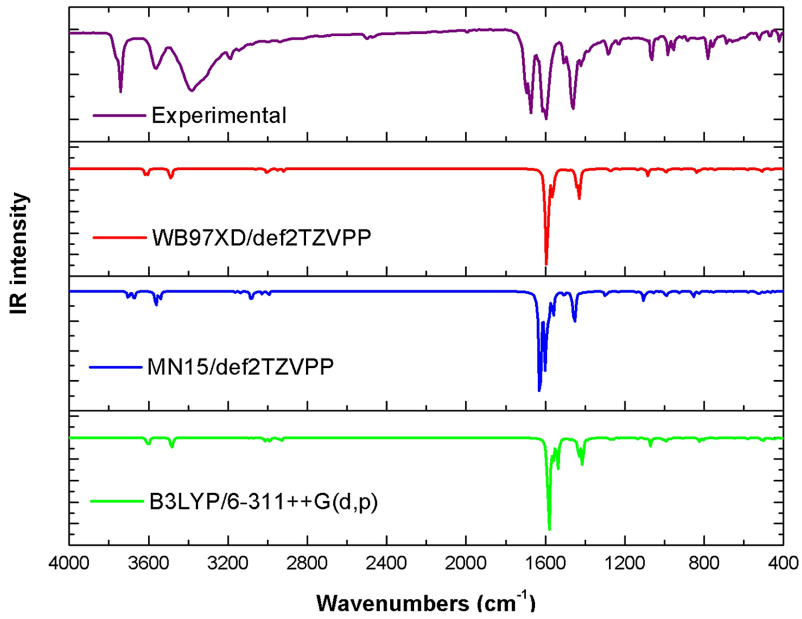

Figure 5. Experimental FT-IR spectra of pyrimethamine.

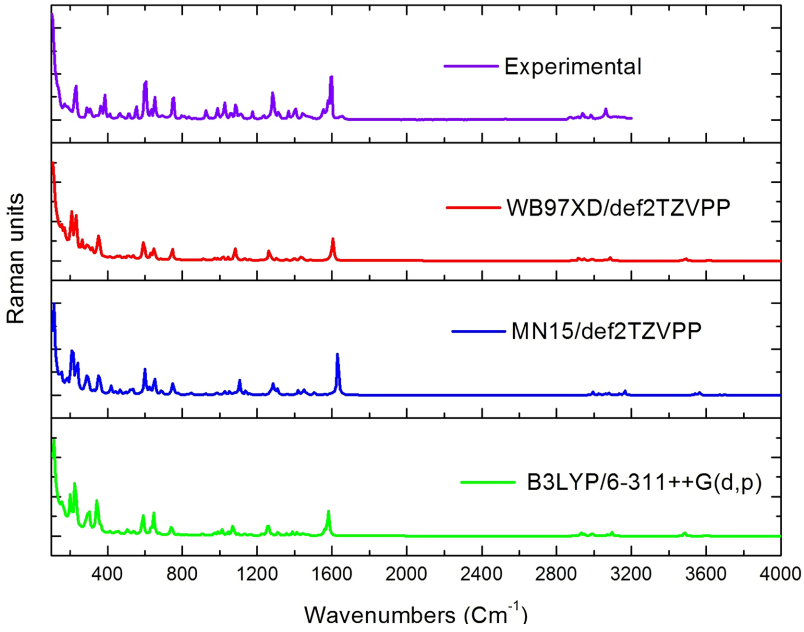

Figure 6. Experimental FT-Raman spectra of pyrimethamine.

The small difference between the experimental and theoretical spectra could be attributed to the fact that experimental results refer to insufficient vibrations in solid phase contrary to gaseous phase.

3.3.1. NH_2 Vibrations

Amino groups are generally known as electron donating groups. They give rise to six internal modes, namely symmetric stretching $\nu_s(NH_2)$, anti-symmetric stretching $\nu_{as}(NH_2)$, scissoring or symmetric deformation or simply deformation $\beta(NH_2)$, anti-symmetric deformations or rocking $\rho(NH_2)$, wagging w(NH_2) and torsion or twist tw(NH_2) modes. For Pyr, the ν_s and ν_{as} modes are localised as pure group modes, whereas the β, ρ, w and tw modes are sometimes mixed with the other ring modes. The NH_2 stretching typically appears in the region 3500 - 3000 cm^{-1} [40]. Two N-H bonds were identified for each NH_2 stretching mode. The experimental N-H stretching vibrations were observed at 3468 and 3310 cm^{-1} in the IR spectrum [41], while the anti-symmetric stretching vibration at 3063 cm^{-1} in the Raman spectrum corresponded to $\nu_{as}(NH_2)$. The lower frequency is assigned to the symmetric (νs) mode and the higher one to the anti-symmetric (ν_{as}) mode. The corresponding anti-symmetric (ν_{as}) stretching vibrations were calculated as 3607 and 3598 cm^{-1} for B3LYP/6-311++G(d,p); 3701 and 3672 cm^{-1} for MN15/def2TZVPP and; 3617 and 3605 cm^{-1} for wB97XD/def2TZVPP, while the symmetric (ν_s) stretching mode were computed as 3485 and 3478 cm^{-1} for B3LYP/6-311++G(d,p); 3562 and 3541 cm^{-1} for MN15/def2TZVPP and, 3491 and 3482 cm^{-1} for wB97XD/def2TZVPP, respectively.

The scissoring modes (β) of the NH_2 group is expected in the range 1625 - 1500 cm^{-1}, which contains a broad and strong IR band with peak at 1628 cm^{-1}. DFT calculations provided values at 1585 and 1577 cm^{-1} for B3LYP/6-311++G(d,p); 1626 and 1622 cm^{-1} for MN15/def2TZVPP and; 1600 and 1592 cm^{-1} for wB97XD/def2TZVPP.

The rocking $\rho(NH_2)$ mode usually appears in the region 1150 - 900 cm^{-1} [40]. Here, the IR band at 1012 cm^{-1} is associated with this mode, were calculated as 1128 and 1067 cm^{-1} for B3LYP/6-311++G(d,p); 1134 and 1085 cm^{-1} for MN15/def2TZVPP and 1128 cm^{-1}, 1592 cm^{-1} for wB97XD/def2TZVPP, respectively.

Twisting tw(NH_2) mode have been obtained at 510, 496 and 475 cm^{-1} for B3LYP/6-311++G(d,p); 522, 512 and 489 cm^{-1} for MN15/def2TZVPP and 515, 502 and 483 cm^{-1} for wB97XD/def2TZVPP, respectively.

Theoretically, wagging w(NH_2) mode appeared at 356, 295 and 287 cm^{-1} for B3LYP/6-311++G(d,p); 353, 280 and 275 cm^{-1} for MN15/def2TZVPP and 350, 291 and 278 cm^{-1} for wB97XD/def2TZVPP, respectively.

3.3.2. C-H Vibrations

The characteristic C-H stretching vibrations of the phenyl rings commonly exhibit multiple weak bands in the region 3100 - 3000 cm^{-1} [40] [41] [42]. The DFT calculations give values at 3094, 3092, 3071 and 3068 cm^{-1} for B3LYP/6-311++G(d,p); 3163, 3162, 3135 and 3133 cm^{-1} for MN15/def2TZVPP and; 3084, 3083, 3060 and 3059 cm^{-1} for wB97XD/def2TZVPP, while the bands were

observed at 3150 and 2985 cm^{-1} in the IR and Raman spectra, respectively. Because of the interaction (sometimes strongly) with various ring C=C vibrations, many bands in the 1600 - 1000 cm^{-1} involve in-plane C-H bending vibrations and 1000 - 700 cm^{-1} in out-plane bending [43], respectively. The C-H in plane bending vibrations of phenyl rings were observed at 1087 cm^{-1} (FTIR spectrum) and 1086 cm^{-1} (Raman spectrum), while calculated ones appeared at 1471, 1371, 1278, 1160 and 1086 cm^{-1} for B3LYP/6-311++G(d,p); 1501, 1393, 1292, 1155 and 1090 cm^{-1} for MN15/def2TZVPP and; 1480, 1377, 1273, 1157 and 1085 cm^{-1} for wB97XD/def2TZVPP, respectively. The C-H out-of-plane bending vibrations of Pyr were observed at 955, 939, 819, and 815 cm^{-1} (B3LYP/6-311++G(d,p)); 974, 972, 849 and 840 cm^{-1} for MN15/def2TZVPP and; 967, 954, 833, and 828 cm^{-1} (wB97XD/def2TZVPP).

3.3.3. CH_2 and CH_3 Vibrations

The vibrations of the CH_2 group, the asymmetric stretch $\nu_{as}CH_2$, the symmetric stretch $\nu_{s}CH_2$ and bending vibrations βCH_2, appear in the region 3000 - 2900 cm^{-1}, 2900 - 2800 cm^{-1} and 1410 - 1480 cm^{-1}, respectively [44] [45]. The νCH_2 stretching vibrations were found at 2977 cm^{-1} in IR spectrum. The DFT calculations gave $\nu_{as}CH_2$ at 3010, 3084 and 3004 cm^{-1} for B3LYP/6-311++G(d,p), MN15/def2TZVPP and wB97XD/def2TZVPP methods, respectively; while $\nu_{s}CH_2$ were found at 2943 (B3LYP), 3026 (MN15) and 2946 cm^{-1} (wB97XD). In the present work, the predicted wavenumbers at 1438 cm^{-1} (B3LYP/6-311++G(d,p)), 1446 cm^{-1} (MN15/def2TZVPP) and 1436 cm^{-1} (wB97XD/def2TZVPP) were identified as CH_2 bending vibrations. For the title molecule, the CH_2 bending mode was observed at 1439 cm^{-1} in FT-IR spectrum. Theoretically, wagging wCH_2 of Pyr was identified at 1306 cm^{-1} (B3LYP/6-311++G(d,p)), 1303 cm^{-1} (MN15/def2TZVPP) and 1297 cm^{-1} (wB97XD/def2TZVPP), while twisting $twCH_2$ were observed at 1221 cm^{-1} (B3LYP/6-311++G(d,p)), 1227 cm^{-1} (MN15/def2TZVPP) and 1217 cm^{-1} (wB97XD/def2TZVPP). The rocking ρCH_2 appeared at 1093 and 774 cm^{-1} (B3LYP/6-311++G(d,p)), 1101 and 770 cm^{-1} (MN15/def2TZVPP) and 1089 and 777 cm^{-1} (wB97XD/def2TZVPP).

The stretching vibrations of the CH_3 group are expected in the range of 2900 - 3050 cm^{-1} [44] [45]. In the present case, the calculated asymmetric stretching modes of the methyl group were found to be: 3010, 2991 and 2985 cm^{-1} for B3LYP/6-311++G(d,p), 3084, 3076 and 3059 cm^{-1} for MN15/def2TZVPP, 3004, 2994 and 2982 cm^{-1} for wB97XD/def2TZVPP while, the symmetric modes were at 2928 cm^{-1} (B3LYP), 2992 cm^{-1} (MN15) and 2917 cm^{-1} (wB97XD). Experimental bands were observed at 2977 cm^{-1} in the IR spectrum and 2985 cm^{-1} for Raman spectrum. The asymmetric and symmetric bending vibrations of the methyl group normally appear in the region of 1400 - 1485 and 1420 - 1380 cm^{-1} [45] [46]. The bands observed at 1479 and 1439 cm^{-1} in the IR spectrum were assigned as CH_3 bending modes. The DFT/B3LYP/wB97XD/MN15 calculations gave the following modes: 1460, 1447 and 1351 cm^{-1} [B3LYP/6-311++G(d,p)]; 1461, 1451 and 1356 cm^{-1} (MN15/def2TZVPP) and; 1447, 1437 and 1356 cm^{-1}

(wB97XD/def2TZVPP).

3.3.4. C=N and C=C Vibrations

The C=N and C=C ring stretching vibrations bands for pyrimidine compounds are often observed with strong absorptions in the region 1600 - 1500 cm^{-1} [47]. In the literature, the vibration bands of C=N and C=C are found at 1650 - 1620 cm^{-1} and 1600 - 1450 cm^{-1}, respectively [48]. In this work, experimental C=N stretching bands at 1560 cm^{-1}, were computed to be 1556 and 1533 cm^{-1} (B3LYP/6-311++G(d,p)), 1589 and 1556 cm^{-1} (MN15/def2TZVPP) and, 1562 and 1551 cm^{-1} (wB97XD/def2TZVPP).

Occurrence of conjugation especially in aromatic rings tends to decrease the frequency of the bond [48]. The C=C stretching vibrations at the α-position of the C=N bond and aromatic ring were observed at 1560 cm^{-1}. The calculated values corresponded to 1575, 1544 and 1533 cm^{-1} (B3LYP/6-311++G(d,p)); 1597, 1589 and 1556 cm^{-1} (MN15/def2TZVPP) and; 1581, 1562 and 1551 cm^{-1} (wB97XD/def2TZVPP).

3.3.5. C-Cl Vibrations

Usually, chlorine present in the molecules has a strong vibration band between 550 and 850 cm^{-1} [49] [50] due to the C-Cl stretching vibrations. In this work, the IR and Raman bands observed at 512 and 475.8 cm^{-1}, respectively, were calculated as 451 cm^{-1} for B3LYP/6-311++G(d,p), 461 cm^{-1} for MN15/def2TZVPP and 457 cm^{-1} for wB97XD/def2TZVPP. The corresponding in-plane deformation modes (bending) appear in the Raman spectrum as a shoulder at 357.3 cm^{-1} while calculated frequencies are identified at 295 cm^{-1} for B3LYP/6-311++G(d,p), 280 cm^{-1} for MN15/def2TZVPP and 291 cm^{-1} for wB97XD/def2TZVPP.

3.4. ^{1}H and ^{13}C NMR Data

The ^{1}H and ^{13}C NMR chemical shifts of the title molecule have been carried out using the B3LYP, MN15 and wB97XD functionals with 6-311++G(d,p), def2TZVPP and def2TZVPP basis sets for the optimized geometry and the results were given in **Table 4** and **Table 5** (see **Figures S3-S5** and **Figures S6-S8** of **Supplementary material** for calculated ^{1}H and ^{13}C NMR spectra, respectively associated to the three methods). The experimental ^{1}H and ^{13}C NMR spectra in DMSO-d_6 (at 600 and 150 MHz, respectively) of the molecule are shown in **Figure S9** and **Figure S10** (**Supplementary material**), respectively. It is noteworthy that the experimental ^{1}H NMR spectrum of the studied compound has been reported in the literature [9].

In the ^{1}H NMR spectra, aromatic ring protons have chemical shifts in the region of 6.5 - 8.0 ppm [51]. From experimental spectrum, we observed the aromatic ring protons between 7.464 and 7.180 ppm. The chemical shifts of the protons were calculated in the region 7.877 - 8.235 ppm for B3LYP/6-311++G(d,p), 8.418 - 8.727 ppm for MN15/def2TZVPP and 8.091 - 8.391 ppm for wB97XD/def2TZVPP. **Table 4** shows some correlations between the experimental and calculated ^{1}H NMR results.

Table 4. Experimental and calculated chemical shifts (in ppm) of isotropic ^{1}H for pyrimethamine under B3LYP/6-311++G(d,p), MN15/def2TZVPP and wB97X-D/def2TZVPP levels.

	Experimental δ_H	B3LYP/6-311++G(d,p)		MN15/def2TZVPP		wB97XD/def2TZVPP	
		σ_{calc}	$\delta_{calc} = \sigma_{TMS} - \sigma_{calc}$ (σ_{TMS} = 32.617)	σ_{calc}	$\delta_{calc} = \sigma_{TMS} - \sigma_{calc}$ (σ_{TMS} = 32.388)	σ_{calc}	$\delta_{calc} = \sigma_{TMS} - \sigma_{calc}$ (σ_{TMS} = 32.214)
H7	7.456	24.388	8.230	23.660	8.727	23.823	8.391
H8	7.463	24.741	7.877	23.970	8.418	24.123	8.091
H9	7.463	24.582	8.035	23.846	8.541	24.006	8.208
H10	7.456	24.382	8.235	23.668	8.720	23.829	8.385
H17	2.087	29.832	2.785	29.552	2.836	29.479	2.735
H18	2.087	29.825	2.792	29.648	2.740	29.488	2.726
H20	0.950	31.271	1.347	31.143	1.245	30.954	1.260
H21	0.950	30.495	2.122	30.314	2.074	30.165	2.049
H22	0.950	31.043	1.574	30.876	1.512	30.720	1.494
H24	5.589	28.643	3.974	28.214	4.174	28.157	4.057
H25	5.589	27.896	4.721	27.405	4.983	27.425	4.789
H27	5.573	27.832	4.785	27.358	5.030	27.366	4.848
H28	5.573	27.731	4.886	27.231	5.157	27.247	4.968

Table 5. Experimental and calculated chemical shifts (in ppm) of isotropic 13C for pyrimethamine under B3LYP/6-311++G(d,p), MN15/def2TZVPP and wB97X-D/def2TZVPP levels.

	Experimental δ_C	B3LYP/6-311++G(d,p)		MN15/def2TZVPP		wB97XD/def2TZVPP	
		σ_{calc}	$\delta_{calc} = \sigma_{TMS} - \sigma_{calc}$ (σ_{TMS} = 186.647)	σ_{calc}	$\delta_{calc} = \sigma_{TMS} - \sigma_{calc}$ (σ_{TMS} = 192.627)	σ_{calc}	$\delta_{calc} = \sigma_{TMS} - \sigma_{calc}$ (σ_{TMS} = 190.622)
C1	135.04	34.166	152.481	21.919	170.708	38.377	152.245
C2	131.79	48.522	138.125	35.480	157.147	51.201	139.421
C3	128.90	45.037	141.610	31.031	161.596	47.242	143.380
C4	132.56	39.822	146.825	24.540	168.086	42.363	148.258
C5	128.90	43.946	142.701	30.181	162.446	46.377	144.245
C6	131.79	48.680	137.968	35.538	157.088	51.262	139.360
C12	105.28	71.914	114.733	62.143	130.483	77.069	113.553
C13	166.49	6.635	180.012	−12.001	204.627	7.578	183.044
C14	161.96	16.440	170.208	0.381	192.246	16.981	173.641
C15	162.15	15.546	171.102	0.807	191.820	16.771	173.851
C16	27.44	150.657	35.990	154.249	38.378	156.174	34.448
C19	13.06	167.550	19.097	173.343	19.284	172.381	18.241
*r	-	-	0.987	-	0.984	-	0.985

*r represents the correlation coefficient between experimental and theoretical data.

In this work, the chemical shifts of the carbon atom in C=N-(C14, C15) found in ^{13}C spectrum of pyrimethamine, were observed at 162.15 and 161.96 ppm and

calculated values at 170.208 and 171.102 ppm for B3LYP/6-311++G(d,p), 173.641 and 173.851 ppm wB97XD/def2TZVPP, 192.246 and 191.820 ppm for MN15/def2TZVPP. As presented in **Table 5**, there is a correlation between the experimental and calculated ^{13}C NMR results, and the corresponding r values were found to be 0.987, 0.985 and 0.984, respectively for corresponding method/basis sets.

3.5. Frontier Molecular Orbitals (HOMO-LUMO)

The most important orbitals in a molecule are the frontier molecular orbitals (FMOs), called highest occupied molecular orbital (HOMO) and lowest unoccupied molecular orbital (LUMO). These orbitals play a significant role in the optical and electric properties, as well as in quantum chemistry, chemical reactions and UV-vis spectra [52]. The energies of HOMO (E_H) and LUMO (E_L) characterize the ability of a molecule to donate and accept electrons, respectively. The difference between E_H and E_L is called energy gap (ΔE_G), which enables the determination of the electrical transport and other properties such as kinetic stability, chemical reactivity, optical polarizability and chemical hardness–softness of the molecular system. The energy gap is large for hard molecules and small for soft molecules [53]. Soft molecules are more polarizable than the hard ones because they need small energy for excitation [54] [55]. The HOMO, LUMO and chemical reactivity descriptors for pyrimethamine were calculated by Gaussian 16 program using B3LYP/6-311++G(d,p), MN15/def2TZVPP and wB97XD/def2TZVPP levels and their values were summarized in **Table 6**.

Calculations indicated that Pyr has 65 occupied sites with high energy gaps found to be 5.015, 6.465 and 8.884 eV ($\Delta E_{HOMO-LUMO}$ gap) with B3LYP/6-311++G(d,p), MN15/def2TZVPP and wB97XD/def2TZVPP methods, respectively and also has high hardness value [2.508 eV (B3LYP), 3.232 eV (MN15) and 4.442 eV (wB97XD)] and low softness value [0.399 eV (B3LYP), 0.309 eV (MN15) and 0.225 eV (wB97XD)]. These results probably suggested that it is a hard molecule with high stability. The 3D plots of HOMO and LUMO orbitals are illustrated in **Figure 7** using B3LYP/6-311++G(d,p) calculation level. The positive and negative phases were represented in red and green colour, respectively.

3.6. Mulliken Atomic Charges

The computation of the reactive atomic charges plays an important role in the application of quantum chemical calculations [56] for the molecular system. The Mulliken atomic charges were calculated by determining the electron population of each atom with DFT using B3LYP, MN15 and wB97XD method at 6-311++G(d,p), def2TZVPP and def2TZVPP basic functions, respectively. The charge distribution calculated by the natural bond orbital (NBO) and Mulliken methods of pyrimethamine are summarized in **Table 7**. From Mulliken charges computation, the carbon atom C15 had a high positive charge compared to all other carbon atoms, because of the three-neighbouring electronegative N26, N29 and

Table 6. Calculated energy values for pyrimethamine under B3LYP/6-311++G(d,p), MN15/def2TZVPP and wB97XD/def2TZVPP levels.

Property	Symbol and formula	B3LYP/6-311++G(d,p)	MN15/def2TZVPP	wB97XD/def2TZVPP
Electronic energy (a.u)	-	−1144.568	−1143.707	−1144.403
HOMO energy (eV)	E_H	−6.074	−6.734	−7.894
LUMO energy (eV)	E_L	−1.059	−0.269	0.990
$\Delta E_{HOMO-LUMO}$ gap (eV)	$\Delta E_G = E_L - E_H$	5.015	6.465	8.884
HOMO+1 energy (eV)	E_{H+1}	−6.664	−7.598	−8.595
LUMO-1 energy (eV)	E_{L-1}	−1.006	−0.194	1.029
$\Delta E_{HOMO-1-LUMO+1}$ gap (eV)	$\Delta E_{G1} = E_{L-1} - E_{H+1}$	5.658	7.405	9.624
Ionization potential (eV)	$I = -E_H$	6.074	6.734	7.894
Electron affinity (eV)	$E_A = -E_L$	1.059	0.269	−0.990
Global hardness (eV)	$\eta = (E_L - E_H)/2$	2.508	3.232	4.442
Chemical reactivity or Global Softness (eV^{-1})	$S = 1/\eta$	0.399	0.309	0.225
Chemical potential (eV)	$\mu = (E_L + E_H)/2$	−3.566	−3.501	−3.452
Electrophilicity index (eV)	$\omega = \mu^2/2\eta$	2.536	1.896	1.341
Electronegativity (eV)	$\chi = -\mu$	3.566	3.501	3.452
Dipole moment (Debye)	D	1.618	1.617	1.616

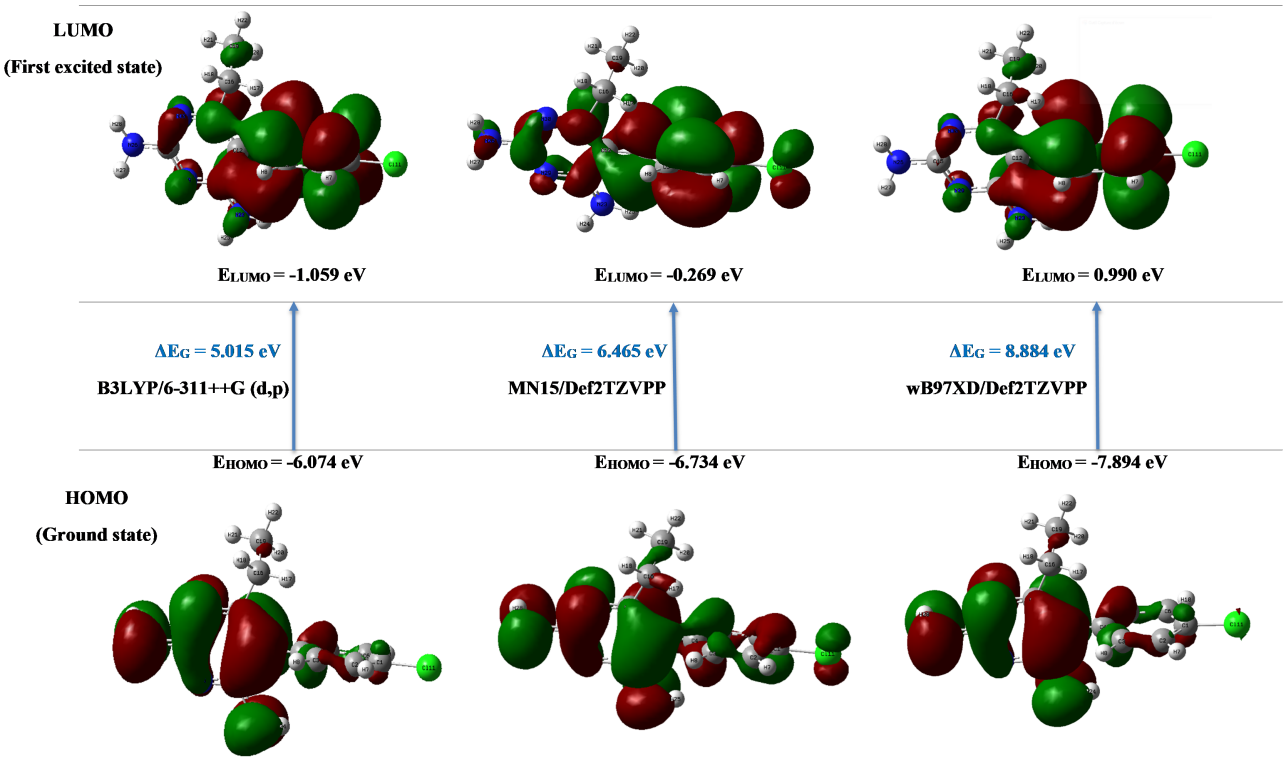

Figure 7. Atomic orbital compositions of the frontier molecular orbital for pyrimethamine.

Table 7. Charge distribution calculated by the natural bond orbital (NBO) and Mulliken methods of pyrimethamine.

Atom number	Atomic charges			Natural charges		
	B3LYP/ 6-311++G(d,p)	MN15/ def2TZVPP	wB97XD/ def2TZVPP	B3LYP/6-311++ G(d,p) Natural	MN15/def2TZVPP Natural	wB97XD/def2TZVPP Natural
C1	0.440381	0.013647	0.125777	−0.0376	−0.02751	−0.02921
C4	0.597027	0.050311	−0.088254	−0.05942	−0.04835	−0.04646
Cl11	0.426522	−0.070622	−0.086846	0.00104	−0.00852	−0.00639
C13	0.09155	0.263542	0.137252	0.29928	0.30301	0.30812
C14	−0.088274	0.176127	0.248832	0.45549	0.43878	0.44416
C15	0.155828	0.195083	0.353153	0.60672	0.5682	0.57236
N23	−0.382647	−0.398026	−0.245656	−0.77367	−0.77722	−0.78115
N26	−0.281552	−0.362795	−0.24894	−0.77831	−0.7767	−0.78137
N29	−0.24011	−0.310812	−0.367737	−0.59712	−0.55409	−0.56243
N30	−0.108056	−0.282251	−0.362885	−0.58878	−0.54878	−0.55406

N30 atoms, respectively. C15 behaves as an acceptor atom and it sustains nucleophilic reactions. The nitrogen atoms N23 and N26 perform as donor atoms, they endure electrophilic reaction. The charge distribution is modified by changing different basis sets as summarized in Table 7. The corresponding Mulliken plots are shown in Figure 8.

3.7. Molecular Electrostatic Potential (MEP) Analysis

The molecular electrostatic potential (MEP) is a very cooperative tool in understanding the relationship between molecular structure and reactivity. MEP mapping is often used for interpretation and prediction of relative reactivity sites for electrophilic and nucleophilic attacks [57] [58], calculations of atomic charges [59], and study of molecular similarity [60].

Three MEP diagrams have been plotted for pyrimethamine at B3LYP/6-311++G(d,p), MN15/def2TZVPP and wB97XD/def2TZVPP levels of calculations as illustrated in Figure 9. This figure provided a visual representation of the chemically active sites and comparative reactivity of atoms. The electrostatic potential increases in the order red < orange < yellow < green < blue, where the blue colour indicates a minimal concentration of electrons (nucleophilic reactivity) and the red indicates a high density of electrons (electrophilic reactivity). In addition, the negative electrostatic potential regions (red) were localized on the carbon atom C15 nearby nitrogen atoms (N26, N29 and N30) indicating possible site for electrophilic attack. However, positive potential regions (blue) were localized around NH_2 groups (N26, N23), indicating possible sites for nucleophilic attack in the drug. This result was also supported by the evidences of charge analysis parts. The docking study by Musa *et al.* [61] reveals that the NH2 group (N26) is the preferred binding site.

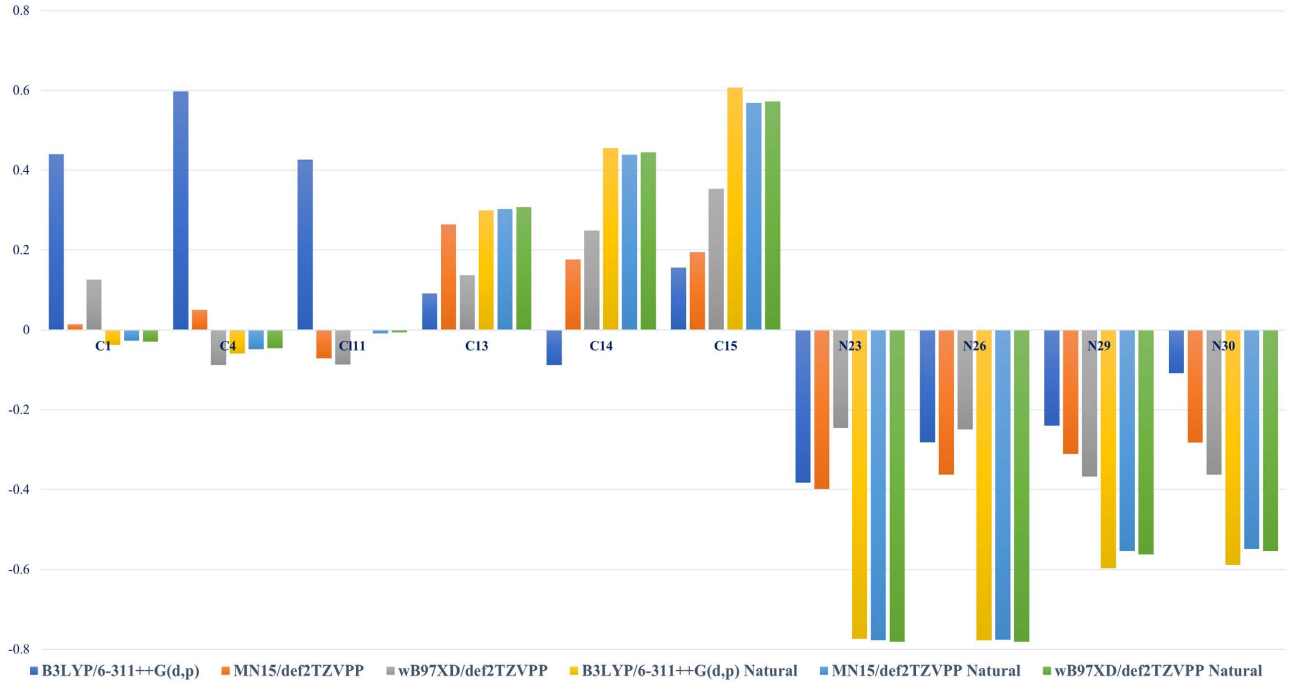

Figure 8. Mulliken atomic charges of pyrimethamine.

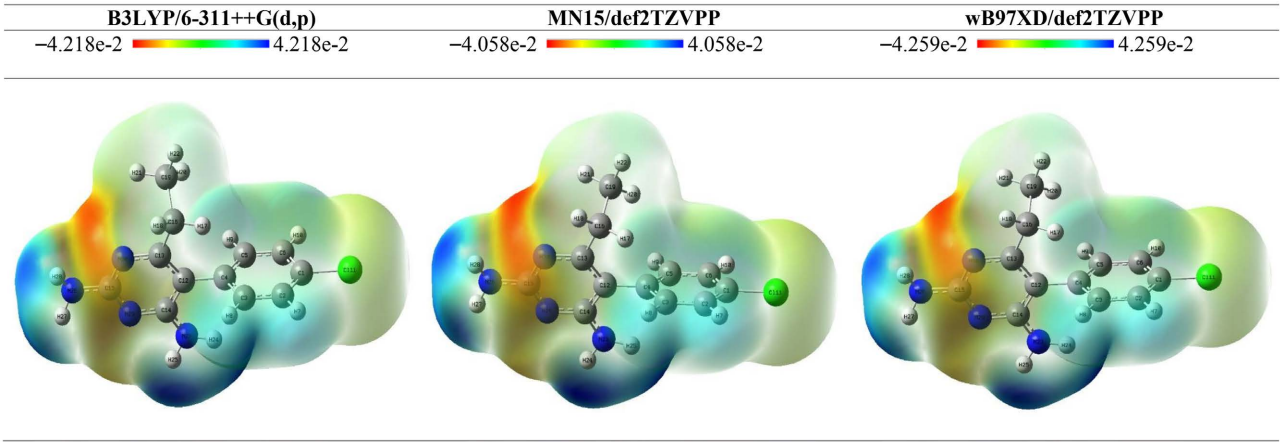

Figure 9. 3D plots of the molecular electrostatic potential map of pyrimethamine.

4. Conclusions

The FT-IR and FT-Raman spectra of pyrimethamine were experimentally studied and analysed, while the X-ray and ^{1}H NMR data were obtained from literature. The molecular geometry and wave numbers were calculated using DFT functionals associated with 6-311++G(d,p) and def2TZVPP basis sets. The optimized geometrical parameters were found to be in good agreement with the XRD results. It is observed that there are no significant differences between the experimental and the theoretical structures. It was noted that some of the experimental results belong to the solid phase, while theoretical calculations were due to gaseous phase. A reasonable agreement was observed between the observed and stimulated spectra (IR and Raman). The TED calculation regarding the

normal modes of vibration provides strong support for the frequency assignment. The spectroscopic investigations showed a high degree of approximation between the calculated and experimental results. However, remarkable differences observed between the experimental and theoretical chemical shifts may be due to the fact that DFT calculations have been performed in the gas phase whereas the experimental results were carried out in solid phase.

The HOMO/LUMO analysis was done in order to characterize the electron density of the molecule. Analysis of Mulliken's charge revealed a concentration of negative charge at the nitrogen atoms of the amino groups, while the carbon atom (C15) is positively charged. The MEP map shows that the negative potential sites are around the carbon atom (C15) and the positive potential sites are on nitrogen atoms of the amino groups. These sites provide information concerning the region from where the molecule can undergo intramolecular and intermolecular interactions.

Overall, the present investigations provide a solid foundation for dealing with diaminopyrimidine compounds.

Acknowledgements

The authors thank the University of Yaoundé I and the Higher Teacher Training College of Yaoundé (Cameroon) for infrastructural facilities.

Conflicts of Interest

The authors declare no conflicts of interest regarding the publication of this paper.

References

[1] Yuthavong, Y. (2013) Antifolate Drugs: Encyclopaedia of Malaria, Vol. 1-12. Springer Science + Business Media, New York. https://doi.org/10.1007/978-1-4614-8757-9_2-1

[2] Nzila, A. (2006) The Past, Present and Future of Antifolates in the Treatment of *Plasmodium falciparum* Infection. *Journal of Antimicrobial Chemotherapy*, **57**, 1043-1054. https://doi.org/10.1093/jac/dkl104

[3] Muller, I.B. and Hyde, J.E. (2013) Folate Metabolism in Human Malaria Parasites—75 Years On. *Molecular and Biochemical Parasitology*, **188**, 63-77. https://doi.org/10.1016/j.molbiopara.2013.02.008

[4] Pierdominici, M., Giammarioli, A.M., Gambardella, L., *et al.* (2005) Pyrimethamine (2,4-Diamino-5-p-chlorophenyl-6-ethylpyrimidine) Induces Apoptosis of Freshly Isolated Human T Lymphocytes, Bypassing CD95/Fas Molecule but Involving Its Intrinsic Pathway. *Journal of Pharmacology and Experimental Therapeutics*, **315**, 1046-1057. https://doi.org/10.1124/jpet.105.086736

[5] Sardarian, A., Douglas, K.T., Read, M., Sims, P.F.G., *et al.* (2003) Pyrimethamine Analogs as Strong Inhibitors of Double and Quadruple Mutants of Dihydrofolate Reductase in Human Malaria Parasites. *Organic & Biomolecular Chemistry*, **1**, 960-964. https://doi.org/10.1039/b211636g

[6] Schwalbe, C.H. and Cody, V. (2006) Structural Characteristics of Small-Molecule

Antifolate Compounds. *Crystallography Reviews*, **12**, 267-300. https://doi.org/10.1080/08893110701337800

[7] Sansom, C.E., Schwalbe, C.H., Lambert, P.A., *et al.* (1989) Structural Studies on Bio-Active Compounds. Part XV. Structure-Activity Relationships for Pyrimethamine and a Series of Diaminopyrimidine Analogues versus Bacterial Dihydrofolate Reductase. *Biochimica et Biophysica Acta*, **995**, 21-27. https://doi.org/10.1016/0167-4838(89)90228-8

[8] Kongsaeree, P., Khongsuk, P., Leartsakulpanich, U., *et al.* (2005) Crystal Structure of Dihydrofolate Reductase from *Plasmodium vivax*: Pyrimethamine Displacement Linked with Mutation-Induced Resistance. *Proceedings of the National Academy of Sciences of the United States of America*, **102**, 13046-13051. https://doi.org/10.1073/pnas.0501747102

[9] Oliveira, S.C. and Figueroa-Villar, J.D. (2002) 1H NMR Spectroscopy Study of the Interaction between Pyrimethamine Hydrochloride and Bovine Serum Albumin. *Journal of Magnetic Resonance*, **1**, 28-31.

[10] Saleh, B.A., Abood, H.A., Miyamoto, R. and Bortoluzzi, M. (2011) Theoretical Study of Substituent Effects on Electronic and Structural Properties of 2,4-Diamino-5-para-substituted-phenyl-6-ethyl-pyrimidines. *Journal of the Iranian Chemical Society*, **8**, 653-661. https://doi.org/10.1007/BF03245897

[11] Sethuraman, V., Stanley, N., Muthiah, P.T., *et al.* (2003) Isomorphism and Crystal Engineering: Organic Ionic Ladders Formed by Supramolecular Motifs in Pyrimethamine Salts. *Crystal Growth & Design*, **3**, 823-828. https://doi.org/10.1021/cg030015j

[12] Stanley, N., Sethuraman, V., Muthiah, P.T., *et al.* (2002) Crystal Engineering of Organic Salts: Hydrogen-Bonded Supramolecular Motifs in Pyrimethamine Hydrogen Glutarate and Pyrimethamine Formate. *Crystal Growth & Design*, **2**, 631-635. https://doi.org/10.1021/cg020027p

[13] Hemamalini, M., Muthiah, P.T., Sridhar, B. and Rajaram, R.K. (2005) Pyrimethamine Sulfosalicylate Monohydrate. *Acta Crystallographica Section E*, **61**, o1480-o1482. https://doi.org/10.1107/S1600536805012237

[14] Tutughamiarsoa, M. and Bolteb, M. (2011) A New Polymorph and Two Pseudo-Polymorphs of Pyrimethamine. *Acta Crystallographica Section C*, **67**, o428-o434. https://doi.org/10.1107/S0108270111038868

[15] Hirao, H., Thellamurege, N. and Zhang, X. (2014) Applications of Density Functional Theory to Iron-Containing Molecules of Bioinorganic Interest. *Frontiers in Chemistry*, **2**, Article No. 14. https://doi.org/10.3389/fchem.2014.00014

[16] Mourik, T., Bühl, M. and Gaigeot, M.P. (2014) Density Functional Theory across Chemistry, Physics and Biology. *Philosophical Transactions of the Royal Society A*, **372**, Article ID: 20120488. https://doi.org/10.1098/rsta.2012.0488

[17] Ravikumar, C., Joe, I.H. and Jayakumar, V.S. (2008) Charge Transfer Interactions and Nonlinear Optical Properties of Push-Pull Chromophore Benzaldehyde Phenylhydrazone: A Vibrational Approach. *Chemical Physics Letters*, **460**, 552-558. https://doi.org/10.1016/j.cplett.2008.06.047

[18] Sun, Y.X., Hao, Q.L., Lu, L.D., *et al.* (2010) Vibrational Spectroscopic Study of o-, m- and p-hydroxybenzylideneaminoantipyrines. *Spectrochimica Acta*, *Part A*: *Molecular and Biomolecular Spectroscopy*, **75**, 203-211. https://doi.org/10.1016/j.saa.2009.10.013

[19] Zalaoglu, Y., Karaboga, F., Yildirim, G., *et al.* (2011) *Ab Initio* Hartree-Fockand Density Functional Theory Study on Characterization of 2-nitro-n-(4-nitrophenyl)

Benzamide. *BPL*, **19**, 137-152.

[20] Sethuraman, V. and Muthiah, P.T. (2002) Hydrogen-Bonded Supramolecular Ribbons in the Antifolate Drug Pyrimethamine. *Acta Crystallographica Section E*, **58**, o817-o818. https://doi.org/10.1107/S1600536802011133

[21] Sethuraman, V. and Muthiah, P.T. (2002) CCDC 193733: Experimental Crystal Structure Determination. https://www.ccdc.cam.ac.uk/structures/Search?Ccdcid=193733&DatabaseToSearch=Published

[22] Becke, A.D. (1993) Density Functional Thermochemistry. III. The Role of Exact Exchange. *The Journal of Chemical Physics*, **98**, 5648-5652. https://doi.org/10.1063/1.464913

[23] Stephens, P.J., Devlin, F.J., Chabalowski, C.F. and Frisch, M.J. (1994) *Ab Initio* Calculation of Vibrational Absorption and Circular Dichroism Spectra Using Density Functional Force Fields. *The Journal of Physical Chemistry*, **98**, 11623-11627. https://doi.org/10.1021/j100096a001

[24] Yu, H.S., He, X., Li, S.L. and Truhlar, D.G. (2016) MN15: A Kohn-Sham Global-Hybrid Exchange-Correlation Density Functional with Broad Accuracy for Multi-Reference and Single-Reference Systems and Noncovalent Interactions. *Chemical Science*, **7**, 5032-5051. https://doi.org/10.1039/C6SC00705H

[25] Weigend, F. (2006) Accurate Coulomb-Fitting Basis Sets for H to Rn. *Physical Chemistry Chemical Physics*, **8**, 1057-1065. https://doi.org/10.1039/b515623h

[26] Chai, J.D. and Gordon, M.H. (2008) Long-Range Corrected Hybrid Density Functionals with Damped Atom-Atom Dispersion Corrections. *Physical Chemistry Chemical Physics*, **10**, 6615-6620. https://doi.org/10.1039/b810189b

[27] Song, J.W., Hirosawa, T., Tsuneda, T. and Hirao, K. (2009) An Improved Long-Range Corrected Hybrid Exchange-Correlation Functional Including a Short-Range Gaussian Attenuation (LCgau-BOP). *The Journal of Chemical Physics*, **131**, Article ID: 059901. https://doi.org/10.1063/1.3202436

[28] Tawada, Y., Tsuneda, T., Yanagisawa, S., *et al.* (2004) A Long-Range-Corrected Time-Dependent Density Functional Theory. *The Journal of Chemical Physics*, **120**, 8425. https://doi.org/10.1063/1.1688752

[29] Chai, J. and Head-Gordon, M. (2008) Systematic Optimization of Long-Range Corrected Hybrid Density Functionals. *The Journal of Chemical Physics*, **128**, Article ID: 084106. https://doi.org/10.1063/1.2834918

[30] Frisch, M.J., Trucks, G.W., Schlegel, H.B., *et al.* (2016) Gaussian 16, Revision B.01. Gaussian, Inc., Wallingford.

[31] Dennington, R., Keith, T. and Millam, J. (2009) Gauss View, Version 5. Semichem Inc., Shawnee Mission.

[32] O'Boyle, N.M., Tenderholt, A.L. and Langner, K.M. (2008) High Capacity Hydrogen Storage in Ni Decorated Carbon Nanocone: A First-Principles Study. *Journal of Computational Chemistry*, **29**, 839-845.

[33] Chamundeeswari, S.P.V., Jebaseelan, E.R.J. and Sundaraganesan, N. (2011) Theoretical and Experimental Studies on 2-(2-methyl-5-nitro-1-imidazolyl) Ethanol. *European Journal of Chemistry*, **2**, 136-145. https://doi.org/10.5155/eurjchem.2.2.136-145.169

[34] NIST (National Institute of Standards and Technology) (2020) Computational Chemistry Comparison and Benchmark Database. NIST Standard Reference Database Number 101 Release 21.

[35] Malloum, A., Fifen, J.J., Dhaouadi, Z., *et al.* (2015) Structures and Relative Stabilities of Ammonia Clusters at Different Temperatures: DFT vs. *Ab-Initio*. *Physical Chemistry Chemical Physics*, **17**, 29226-29242. https://doi.org/10.1039/C5CP03374H

[36] Jamroz, M.H. (2013) Vibrational Energy Distribution Analysis (VEDA): Scopes and Limitations. *Spectrochimica Acta*, *Part A*: *Molecular and Biomolecular Spectroscopy*, **114**, 220-230. https://doi.org/10.1016/j.saa.2013.05.096

[37] Krzysztof, W., James, F.H. and Pulay, P.J. (1990) Efficient Implementation of the Gauge-Independent Atomic Orbital Method for NMR Chemical Shift Calculations. *Journal of the American Chemical Society*, **112**, 8251-8260. https://doi.org/10.1021/ja00179a005

[38] Jian, F.F., Zhao, P.S., Bai, Z.S. and Zhang, L. (2005) Quantum Chemical Calculation Studies on 4-phenyl-1-(propan-2-ylidene) Thiosemicarbazide. *Structural Chemistry*, **16**, 635-639. https://doi.org/10.1007/s11224-005-8254-z

[39] Dabbagh, H.A., Zamani, M., Farrokhpour, H., *et al.* (2010) Conformational Analysis and Intramolecular/Intermolecular Interactions of N,N'-dibenzylideneethylenediamine Derivatives. *Journal of Molecular Structure*, **983**, 169-185. https://doi.org/10.1016/j.molstruc.2010.08.048

[40] Stuart, B.H. (2004) Infrared Spectroscopy: Fundamentals and Applications. Vol. 1-244, Wiley & Sons Ltd., Chichester. https://doi.org/10.1002/0470011149

[41] Karrouchi, K., Brandán, S.A., Sert, Y., *et al.* (2020) Synthesis, X-Ray Structure, Vibrational Spectroscopy, DFT Investigation, Biological Evaluation and Molecular Docking of (E)-N'-(4-(dimethylamino)benzylidene)-5-methyl-1H-pyrazole-3-carbohydrazide. *Journal of Molecular Structure*, **1219**, Article ID: 128541. https://doi.org/10.1016/j.molstruc.2020.128541

[42] Onyeji, C.O., Omoruyi, S.I., Oladimeji, F.A. and Soyinka, J.O. (2009) Physicochemical Characterization and Dissolution Properties of Binary Systems of Pyrimethamine and 2-Hydroxypropyl-β-cyclodextrin. *African Journal of Biotechnology*, **8**, 1651-1659.

[43] Lin-Vien, D., Colthup, N.B., Fateley, W. and Grasselli, J. (1991) The Handbook of Infrared and Raman Characteristic Frequencies of Organic Molecules. Elsevier, Amsterdam, 277-306. https://doi.org/10.1016/B978-0-08-057116-4.50023-7

[44] Sajan, D., Binoy, J., Pradeep, B., *et al.* (2004) NIR-FT Raman and Infrared Spectra and *Ab Initio* Computations of Glycinium Oxalate. *Spectrochimica Acta*, *Part A*: *Molecular and Biomolecular Spectroscopy*, **60**, 173-180. https://doi.org/10.1016/S1386-1425(03)00193-8

[45] Roeges, N.P.G. (1994) A Guide to the Complete Interpretation of Infrared Spectra of Organic Structures. Vol. 1-360, Wiley and Sons Inc., New York.

[46] Socrates, G. (1980) Infrared Characteristic, Infrared Characteristic Group Frequencies. Vol. 1-174, Wiley & Sons, Chichester. https://doi.org/10.1016/0022-2860(81)85280-5

[47] Al-Omary, F.A.M., Raj, A. and Raju, K. (2015) Spectroscopic Investigation (FT-IR, FT-Raman), HOMO-LUMO, NBO Analysis and Molecular Docking Study of 2-[(4-chlorobenzyl)sulfanyl]-4-(2-methylpropyl)-6-[3-trifluoromethyl)-anilino]pyrimidine-5-carbonitrile, a Potential Chemotherapeutic Agent. *Spectrochimica Acta*, *Part A*: *Molecular and Biomolecular Spectroscopy*, **136**, 520-533. https://doi.org/10.1016/j.saa.2014.09.066

[48] Yadav, L.D.S. (2013) Organic Spectroscopy. Vol. 1-334, 2004th Edition, Springer, Berlin.

[49] Kurt, M., Yurdakul, M. and Yurdakul, S. (2004) Molecular Structure and Vibrational Spectra of 3-Chloro-4-methyl Aniline by Density Functional Theory and *Ab Initio* Hartree-Fock Calculations. *Journal of Molecular Structure*, *THEOCHEM*, **711**, 25-32. https://doi.org/10.1016/j.theochem.2004.07.034

[50] Romano, E., Davies, L. and Antonia Brandán, S. (2017) Structural Properties and FTIR-Raman Spectra of the Anti-Hypertensive, Clonidine Hydrochloride Agent and Their Dimeric Species. *Journal of Molecular Structure*, **1133**, 226-235. https://doi.org/10.1016/j.molstruc.2016.12.008

[51] Anderson, R.J., Bendell, D.J. and Groundwater, P.W. (2004) Organic Spectroscopic Analysis. *Journal of Natural Products*, **67**, 2158.

[52] Fleming, I. (1976) Frontier Orbitals and Organic Chemical Reactions. Vol. 1-249, Wiley, London.

[53] Mathammal, R., Jayamani, N. and Geetha, N. (2013) Molecular Structure, NMR, HOMO, LUMO, and Vibrational Analysis of O-Anisic Acid and Anisic Acid Based on DFT Calculations. *Journal of Spectroscopy*, **2013**, Article ID: 171735. https://doi.org/10.1155/2013/171735

[54] Kosar, B. and Albayrak, C. (2011) Spectroscopic Investigations and Quantum Chemical Computational Study of (E)-4-methoxy-2-[(p-tolylimino)methyl]phenol. *Spectrochimica Acta*, *Part A*: *Molecular and Biomolecular Spectroscopy*, **78**, 160-167. https://doi.org/10.1016/j.saa.2010.09.016

[55] Obi-Egbedi, N.O., Obot, I.B. and El-Khaiary, M.I. (2011) Quantum Chemical Investigation and Statistical Analysis of the Relationship between Corrosion Inhibition Efficiency and Molecular Structure of Xanthene and Its Derivatives on Mild Steel in Sulphuric Acid. *Journal of Molecular Structure*, **1002**, 86-96. https://doi.org/10.1016/j.molstruc.2011.07.003

[56] Gunasekaran, S., Kumaresan, S., Arunbalaji, R., *et al.* (2008) Density Functional Theory Study of Vibrational Spectra, and Assignment of Fundamental Modes of Dacarbazine. *Journal of Chemical Sciences*, **120**, 315-324. https://doi.org/10.1007/s12039-008-0054-8

[57] Murray, J.S. and Sen, K. (1996) Molecular Electrostatic Potentials: Concepts and Applications. In: *Theoretical and Computational Chemistry*, Vol. 3, Elsevier Science, Amsterdam, 1-665.

[58] Erfu, H., Siyamak, S., Sultan, A.S., *et al.* (2021) Quantum Chemical Modeling, Synthesis, Spectroscopic (FT-IR, Excited States, UV-Vis) Studies, FMO, QTAIM, NBO and NLO Analyses of Two New Azo Derivatives. *Journal of Molecular Structure*, **1243**, Article ID: 130810. https://doi.org/10.1016/j.molstruc.2021.130810

[59] Cox, S.R. and Williams, D.E. (1981) Representation of the Molecular Electrostatic Potential by a Net Atomic Charge Model. *Journal of Computational Chemistry*, **2**, 304-323. https://doi.org/10.1002/jcc.540020312

[60] Carbó, R. and Calabuig, B. (1989) Molsimil-88: Molecular Similarity Calculations Using a CNDO-Like Approximation. *Computer Physics Communications*, **55**, 117-126. https://doi.org/10.1016/0010-4655(89)90070-2

[61] Musa, K.A., Ning, T., Mohamad, S.B. and Tayyab, S. (2020) Intermolecular Recognition between Pyrimethamine, an Antimalarial Drug and Human Serum Albumin: Spectroscopic and Docking Study. *Journal of Molecular Liquids*, **311**, Article ID: 113270. https://doi.org/10.1016/j.molliq.2020.113270

Supplementary Material

Supporting data have been provided herein.

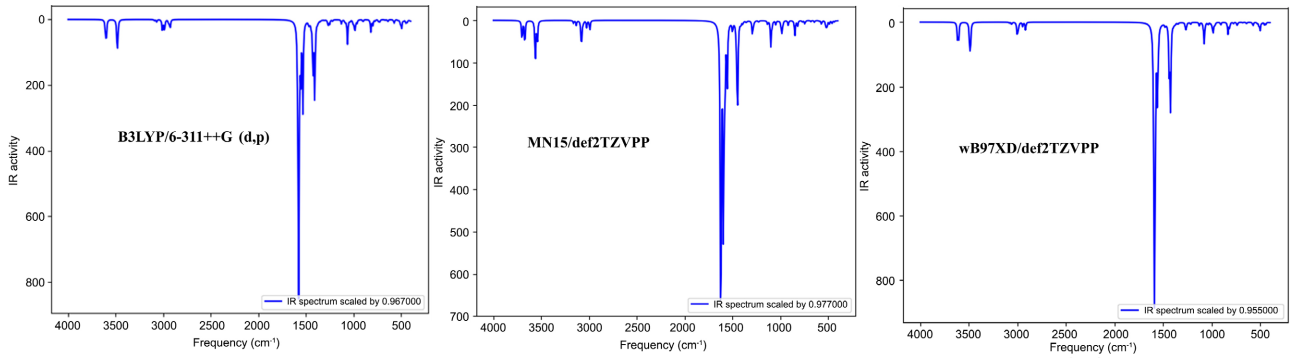

Figure S1. Theoretical FT-IR spectra of pyrimethamine.

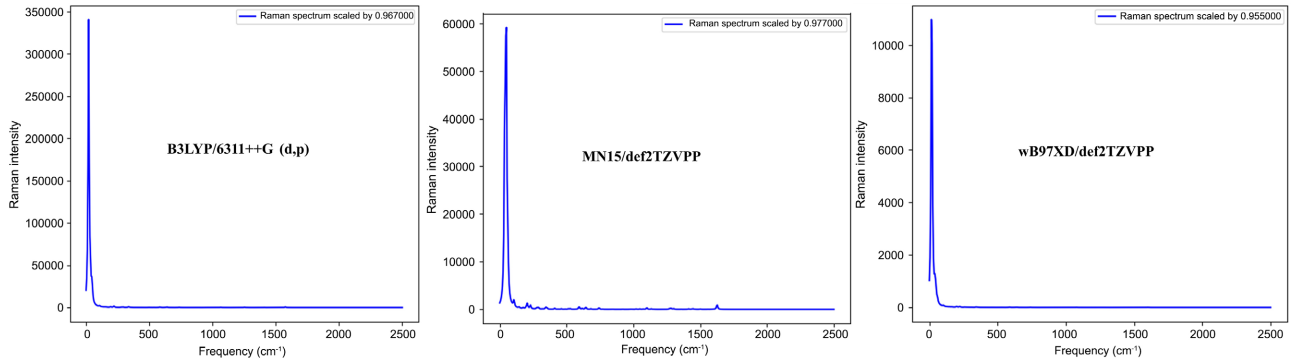

Figure S2. Theoretical FT-Raman spectra of pyrimethamine.

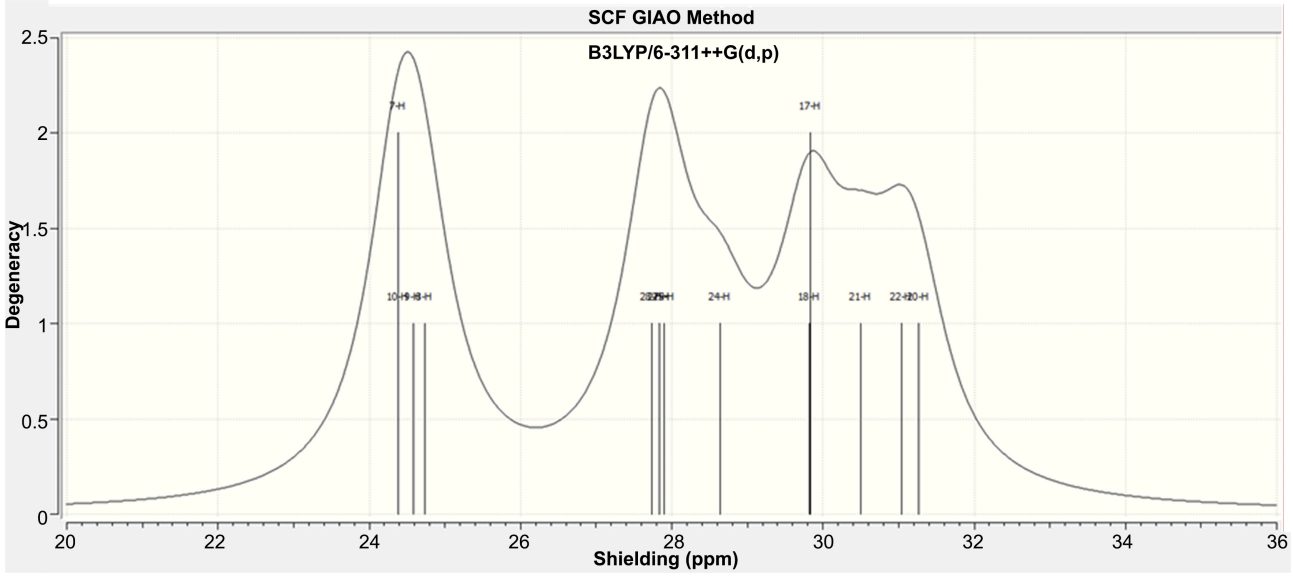

Figure S3. Theoretical ^{1}H NMR spectrum of pyrimethamine by DFT/B3LYP/6-311++G(d,p).

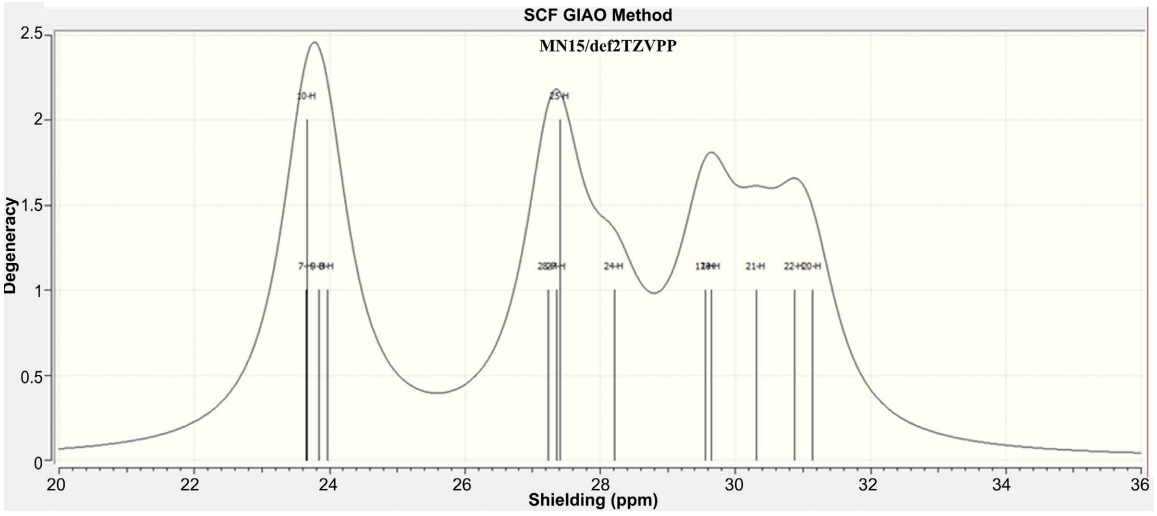

Figure S4. Theoretical ^{1}H NMR spectrum of pyrimethamine by DFT/MN15/def2TZVPP.

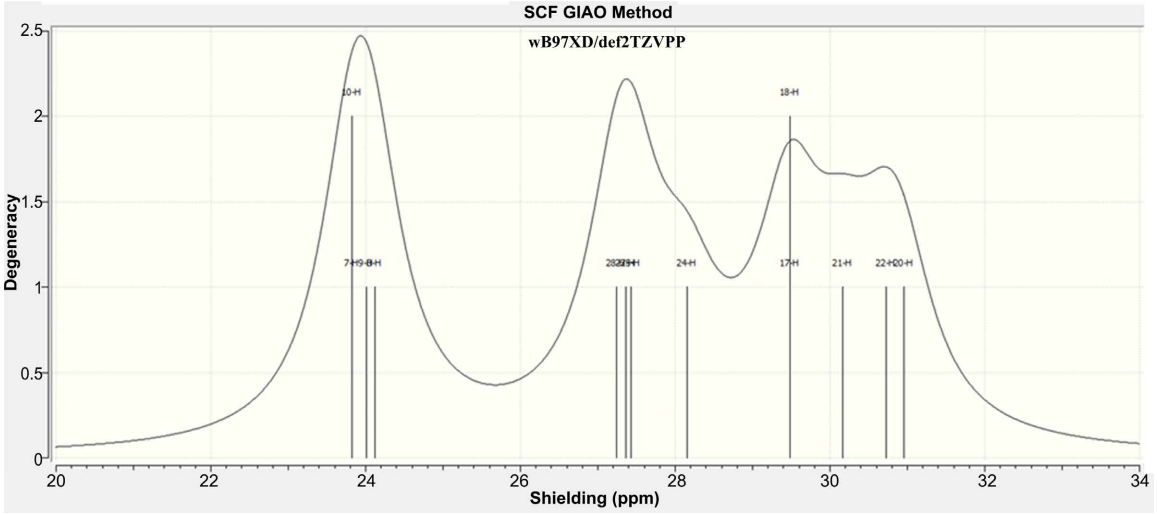

Figure S5. Theoretical ^{1}H NMR spectrum of pyrimethamine by DFT/wB97XD/def2TZVPP.

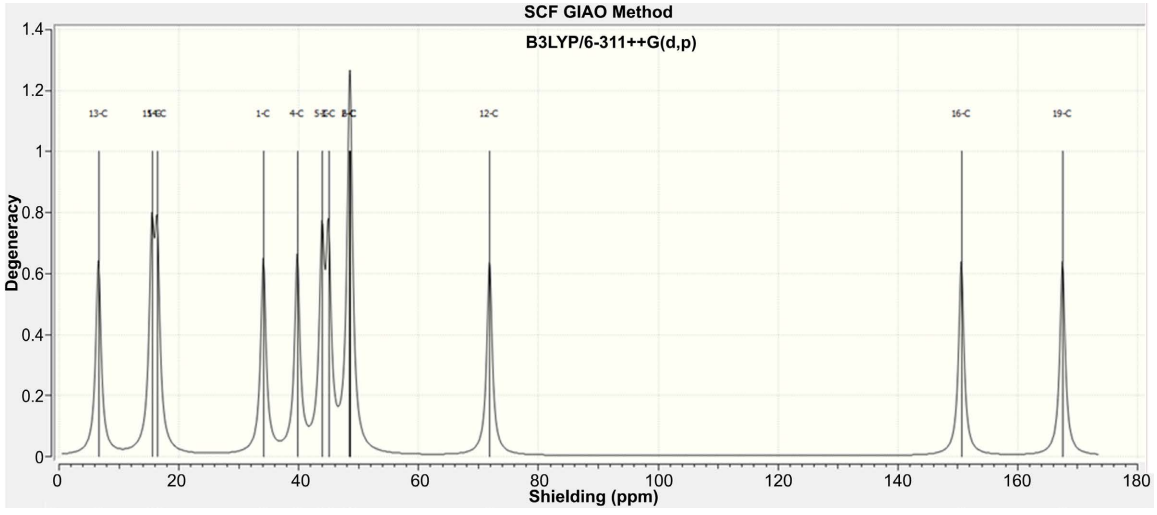

Figure S6. Theoretical ^{13}C NMR spectrum of pyrimethamine by DFT/B3LYP/6-311++G(d,p).

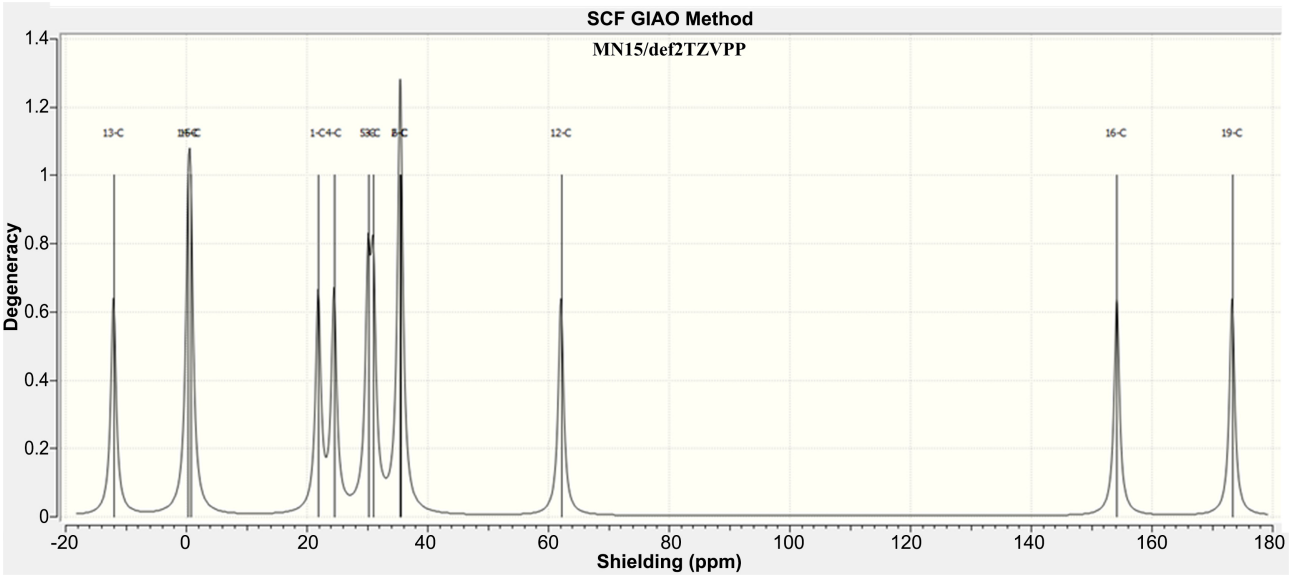

Figure S7. Theoretical ^{13}C NMR spectrum of pyrimethamine by DFT/MN15/def2TZVPP.

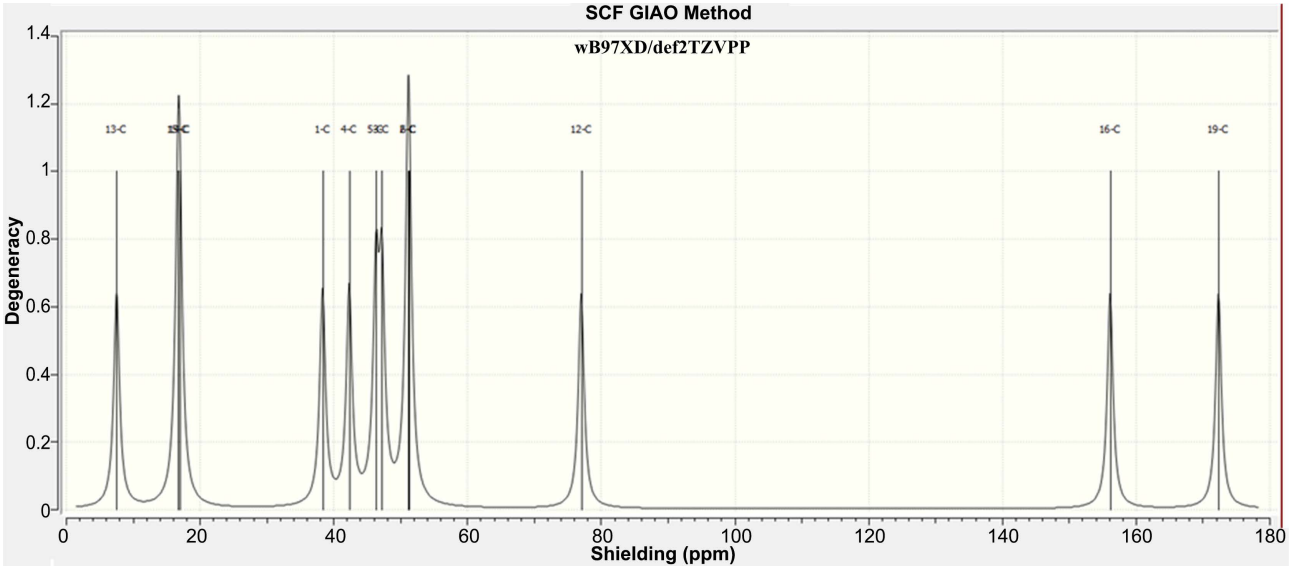

Figure S8. Theoretical ^{13}C NMR spectrum of pyrimethamine by DFT/wB97XD/def2TZVPP.

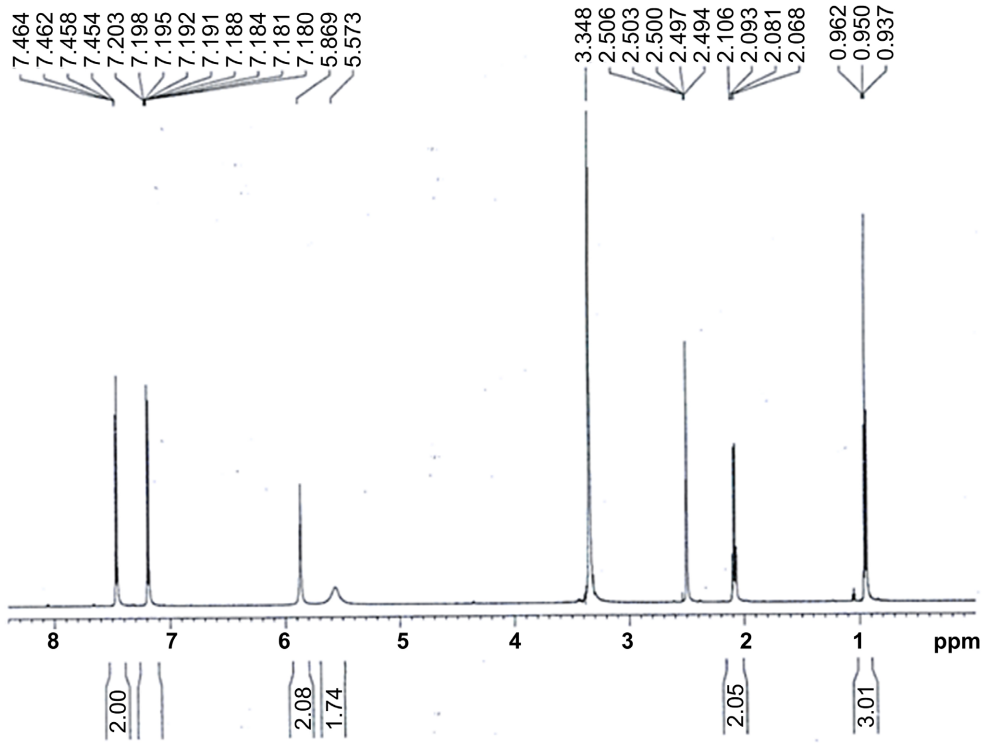

Figure S9. Experimental ^{1}H NMR spectrum (600 MHz, DMSO) of pyrimethamine.

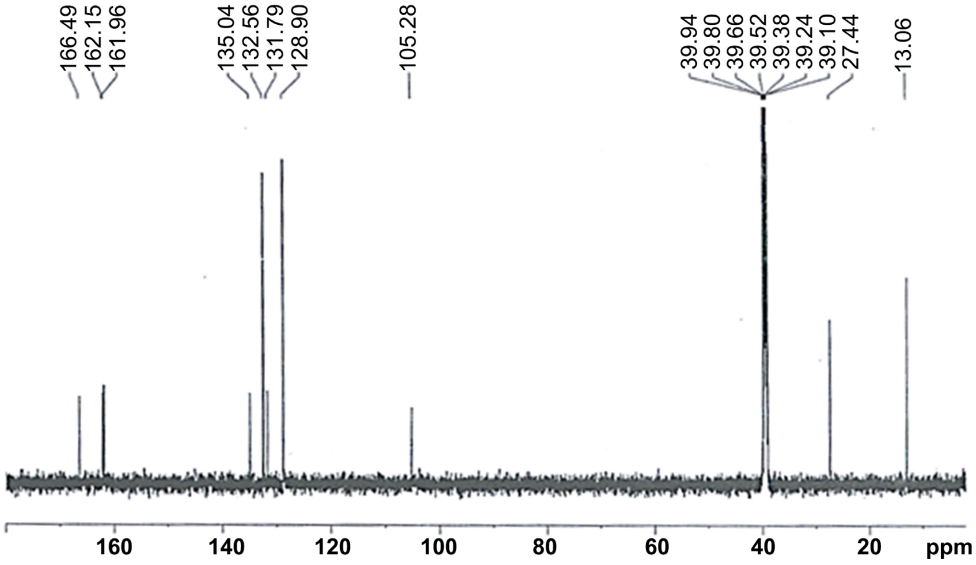

Figure S10. Experimental ^{13}C NMR spectrum (150 MHz, DMSO) of pyrimethamine.